GLAST Prototype Tray and Ladder Thermal Test Report

Mike Steinzig, Erik Swensen, Steve Ney
5/9/2000

	Name:	Phone:	Signature:
Main Author:	Mike Steinzig	(505) 662-0507	
Approved:	Erik Swensen	(505) 661-4021	

Abstract

The primary purpose of these tests was to validate finite element (FE) models of the Tracker Tray and to investigate the response of different face sheet materials to thermal fluctuations. Two different test assemblies were developed to make this comparison; the first was a prototype of a GLAST Tracker Tray, the second were strips of silicon mounted on ladders comprised of several different face sheets for comparison. Measured strain for each test was compared to FE predictions developed at HYTEC, Inc. Thermal testing subjected the tracker tray and the strips to operating temperatures and survival temperatures prescribed for the GLAST instrument. Silicon detectors were broken in both the tray and ladder tests, and are attributed to epoxy failures. Epoxy failure includes de-bonding as well as the epoxy softening that occurs because of a glass transition temperature.

Required input to the FE model is the silicon coefficient of thermal expansion (CTE), which was determined as a function of temperature using the strain gage method. The measured CTE for silicon compared favorably with handbook data.

DESIGN ENGINEERING
ADVANCED COMPOSITE APPLICATIONS
ULTRA-STABLE PLATFORMS

110 EASTGATE DR.
LOS ALAMOS, NM 87544

PHONE 505 661•3000
FAX 505 662•5179
WWW.HYTECINC.COM

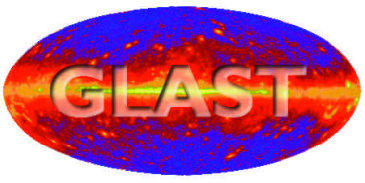

Revision Log

Rev.	Date	Author(s)	Summary of Revisions/Comments
-	05/09/2000	MLS	Initial release.

Table of Contents

1. Summary and Future Activities

1.1 Tracker tray and ladder strip test results

The objective of these tests is to determine whether the tracker tray assembly can withstand the thermal environment to which the GLAST instrument will be subjected. A major concern is the coefficient of thermal expansion (CTE) mismatch between the lead converter sheets, which have a CTE of about 29 ppm/°C, and the silicon detectors, which have a CTE of about 2.5 ppm/°C. This mismatch will develop large stresses in the detectors, possibly leading to failure at the operating or survival temperatures. The proposed solution to this problem is to utilize a face sheet with a negative CTE to reduce the overall CTE to an acceptable level. HYTEC, Inc.'s report titled "Tracker Thermal Test Plan" [1]describes the setup and procedure for taking strain measurements of the prototype Tracker Tray Assembly (referred to in this report as tray tests). A similar procedure was followed to test various face sheet materials that will be used to support the silicon, referred to in this report as ladder tests. The ladder tests also utilized live detectors to monitor the leakage current and indicate when failure occurred.

The tray was tested over operational (40 to -10°C) and survival (60 to -55°C) temperature ranges, which were defined in the Interface Requirements Document[2]. Two obvious catastrophic failures of the detectors occurred during the cyclic tests. These failures are attributed to the CTE mismatch between the lead and the silicon. Localized stress levels appeared to be magnified by the de-bonding of some of the epoxy pads used to attach the silicon to the kapton. The de-bondings resulted in longer unsupported lengths of silicon, allowing greater out-of-plane bending and the eventual fracture of the adjacent detector. It appears that some of the debondings may have occurred at temperatures as high as 3°C. The tray test will be discussed in detail in Section 3.

The ladder tests were meant to validate analytical models, which show that the CTE mismatch can be substantially reduced by using a face sheet material with a near zero CTE, such as graphite/cyanate ester (Gr/CE). By properly designing the thickness of the face sheet, and bonding it to the lead converter, the effective CTE of the payload can be reduced to an acceptable level. To this end, four ladder assemblies were made using 1) thick carbon face sheet, 2) thin carbon face sheet, 3) aluminum face sheet, and 4) a thick lead converter (SuperGLAST) layer with a thick carbon face sheet. The ladders were bonded to a HEXCEL aluminum honeycomb core, which was in turn bonded to a 1" thick aluminum plate. The ladders were tested over an operating temperature range (40 to -10°C) and a revised survival temperature range (60 to -23°C).

It was found during the ladder tests that the honeycomb is sufficiently strong in shear to transmit much of the expansion/contraction of the 1" thick aluminum mounting plate into the ladders. The ladder test results are therefore overshadowed by the effect of the aluminum tooling plate, and do not provide direct information about how the various face sheet materials performed in reducing overall strains in the detectors. Three modes of failure were observed during the ladder tests. The first included definite evidence of a glass transition temperature of the epoxy that occurred at around 50°C. Evidence of the transition is shown by the measurement

of zero strain at all locations for test temperatures of 50°C and 60°C. The epoxy re-cured at lower test temperatures, which built up a residual stress in the detectors, and probably contributed to the failures observed later at lower temperatures. The second failure mechanism is de-bonding of the epoxy pads. This is believed to have occured at about -3°C, but is obviously dependent on the stress, which varies with location. De-bondings were evident in all four ladders. The third is the fracture of a silicon detector. The first catastrophic failure occurred at about -21°C, as determined by a leakage current spike. However, the location of the failure was not identified. Two more catastrophic failures occurred during the last stages of the testing below -21°C. The ladder test will be discussed in more detail in Section 4.

1.2 Conclusions

Both the tray and ladder tests have shown that the epoxy plays an important role in the integrity of the structure. The de-bonding and subsequent failures are a direct result of the CTE mismatch between the lead converter and the silicon detectors. Analysis predicts that with an aluminum face sheet, the CTE mismatch will cause normal stresses very near to the expected failure limit for silicon, even if de-bonding does not occur. The proposed method for eliminating this mismatch is to tailor the effective CTE of the ladder assembly to match that of silicon by bonding a low or negative CTE material to the lead converter. This method has some proven history, but still needs to be demonstrated by testing on the specific layup of interest to the GLAST program.

By reducing the CTE mismatch, the inter-laminar shear stress on the epoxy bonds will be substantially reduced, eliminating the potential for the stress induced de-bonding noticed in both the tray and ladder tests. It has also been proposed that continuous bonding of the silicon to the kapton be used to eliminate the catastrophic damage that was observed in the tray and ladder tests when a bond fails. It is believed that the continuous bond does provide a better method for attaching the silicon to the kapton, because the increased bonding area decreases the likelihood of a de-bonding in the first place. This continuous bonding option will not, however, eliminate the high normal stresses in the silicon that are a result of the CTE mismatch. HYTEC, Inc. believes the continuous bonding should be investigated through modeling and testing in conjunction with ladder assembly designs that reduce the CTE mismatch.

A second issue that needs to be addressed is the glass transition temperature of the epoxy. If the overall CTE is very small, the glass transition effects are minimized as far as stresses are concerned, whether the silicon bonding is continuous or discreet. However, the structural integrity of the assembly will be questionable, and dynamic failures could occur.

1.3 Future activities to solve payload design issues

The tray test and ladder test have been very successful in providing insight into the various modes of failure the tracker can expect to encounter with the current tray/payload design, as well as providing a means to validate FE models used to investigate the CTE mismatch between the silicon detectors and the lead converters. It was hoped that failure limit stress levels for the silicon would be measured during the ladder tests, but a minor oversight in the test coupon design lead to an amplification of the measured stress levels that will not be experienced in the actual thermal environment. The silicon failure limit stress levels being used currently are based on previous HYTEC, Inc. experience, but actual values must be acquired by future testing.

To ensure that a cost efficient payload attachment design is developed in a timely manner, HYTEC is recommending that a specific design and test plan is followed. The design sequence must include all aspects of the payload attachment design, from material selection to laminate design to epoxy specification and bond pad thickness requirements. The tests have shown that pad de-bonding and exceeding the glass transition temperature can be disastrous to the tracker, which indicates that both the method of attachment and the specific epoxy used to attach the silicon detectors to the kapton bias ply (as well as silicon to silicon edge bonds) require a well defined design effort. This effort would include a detailed design phase to investigate various attachment methods and identify acceptable edge and mounting pad epoxies/silicon, followed by a testing phase to validate specific design choices and requirements. The design and testing phase must include numerical simulations to validate both the design and the test coupons to ensure specific design variables are being measured during coupon testing. Trial-and-error testing is very inefficient and time consuming.

The next phase of design would address payload attachment to the tray as well as the CTE mismatch issues discussed herein. There are a number of viable solutions that must be investigated and all design issues must be addressed to ensure the optimal solution is implemented. The design phase would investigate material selection of the tray face sheets and core, size tray components to avoid collisions with adjacent trays during the dynamic environment of launch, and address CTE mismatch issues when laminating the lead converter layer and silicon payload (SuperGLAST is most critical here). A series of specific coupon tests will be required to verify design choices. These tests may include, but are not limited to, pull tests to validate the silicon ultimate strength, dynamic testing of a single tray to verify random vibration response during launch, two point bend testing of composite honeycomb to determine material properties, and thermal testing of Gr/CE/Pb converter laminate coupons to validate mechanical characteristics and manufacturability.

Numerical simulations of each proposed test are essential to ensure specific experimental goals are obtained during testing, without building a test prototype of an entire assembly. For example, 2D (through thickness and parallel to ladder axis) single ladder coupon samples could be fabricated to measure the failure limit of the silicon payload. However, without testing an assembly that includes the tray closeout, stiffening effects from membrane stresses are not present, and thus the measured strains will be larger than in the actual design. A numerical simulation of the entire tray and closeout would show this stiffening effect, and could be compared to another simulation of the individual ladders. This comparison would thus show the magnitude of the stiffening effect, and allow the test designer to make a conscious decision about whether it could be ignored or must be accounted for by modifying the test prototype. This is only an example of the benefit of numerical simulations, but it shows the potential for saving time and money in the testing procedure, and the utility in increasing the level of understanding in the test data. It is HYTEC's opinion that numerical simulations are an essential part of a testing plan for these reasons.

HYTEC has been funded to perform a small portion of these tasks and is currently addressing such issues. Additional tasks would expand the scope of the current HYTEC work to develop and implement a detailed design & test plan with specific goals in mind to ensure project milestones are being met.

2. Measurement of Silicon CTE

Published data on silicon CTE is available in the expected temperature range. However, independently measuring the CTE will verify the test setup and instrumentation at HYTEC, Inc. In addition, the tests will allow determination of anisotropic CTE's that may exist because of the single-crystal makeup of the silicon detectors.

2.1 Test Method and Data Reduction

The dilatometer is the classical means for measuring CTE, but requires very exacting procedures and equipment. A less demanding method is to use two well-matched strain gages. This method is outlined here, but is fully described by Vishay.[3]

One strain gage is bonded to a reference material, (titanium-silicate in this case) for which the CTE is known as a function of temperature. A second gage is bonded to the sample. The known expansion characteristics for the reference material make it possible to calculate the CTE of the sample using the following formula

$$a_S = \frac{e_{Sm} - e_{Rm}}{\Delta T} + a_R \qquad (1)$$

where the S and R subscripts refer to the sample (silicon) and reference (titanium–silicate) materials, respectively, and the subscript m refers to measured. The CTE is α, and the thermal output is ε, as measured by the strain gages over a specific temperature change ΔT. To make the conversion of measured temperature and strain data convenient, we rewrite the equation above as

$$a_S = \frac{d}{dT}(e_{Sm} - e_{Rm}) + \frac{d}{dT}e_R \qquad (2)$$

Values of e_R are obtained from the Vishay technical note mentioned above, and is the actual temperature dependent thermal strain of titanium silicate. Next we need $e_{Sm} - e_{Rm}$, the difference in thermal output between the silicon and reference material. Thermal output is defined as the temperature induced apparent strain of a gage mounted to a stress free material when the temperature is subsequently changed. The thermal output is caused by two factors: 1) the resistivity of the grid alloy changes as a function of temperature, and 2) the resistance changes because of the CTE mismatch between the gage and the material to which it is mounted, which induces a mechanical strain. Algebraically, it can be shown that these effects can be combined in Equation 2 to solve for the CTE of the sample material by simply measuring the thermal output of a sample and a reference material under the same conditions. The thermal output for the reference material is plotted in Figure 1, which also shows the 2nd order polynomial fit to the data. Figure 2 shows the value $e_{Sm} - e_{Rm}$ for both longitudinal and transverse gages, and the 2nd order curves fit to the data.

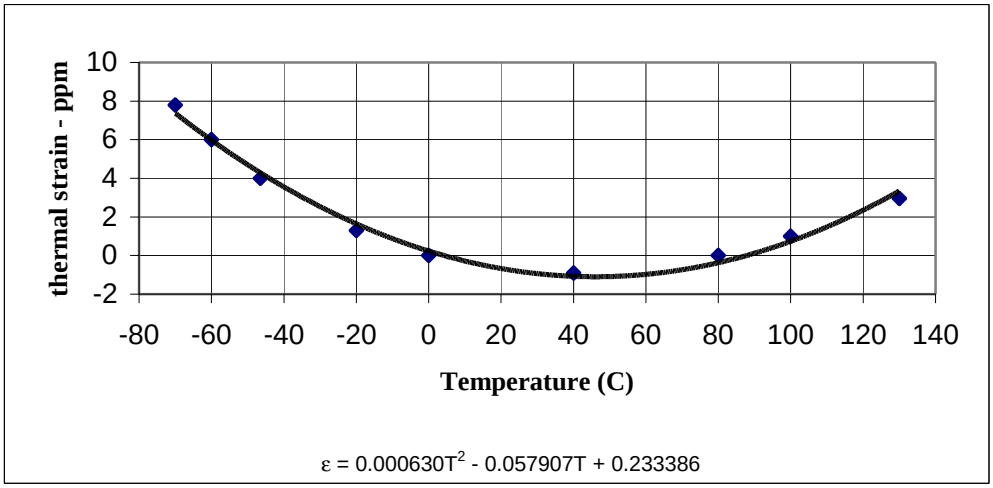

Figure 1: Titanium-silicate reference curve from Vishay tech notes

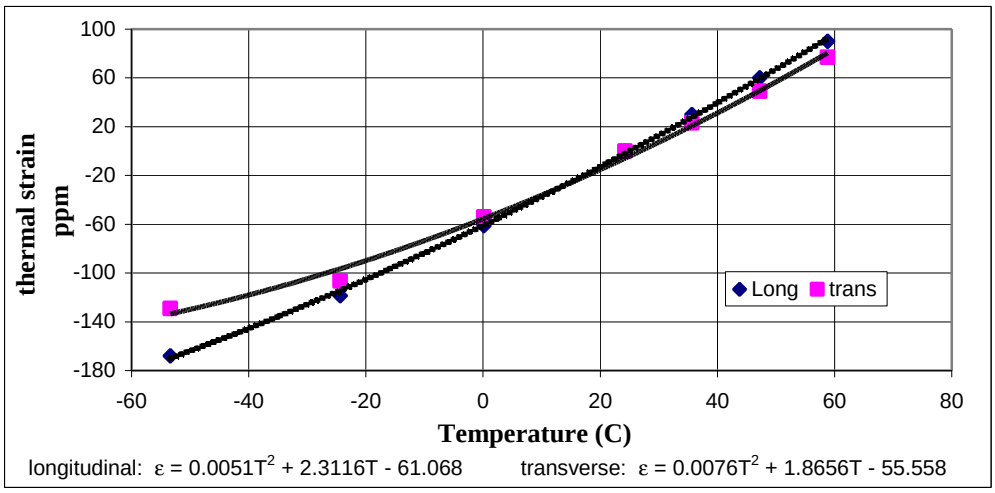

Figure 2: Difference in measured strain $e_{Sm} - e_{Rm}$ for the silicon and titanium silicate reference

The equations of the curves are then differentiated and used in Equation 2 to solve for the CTE's, to give the following expressions.

$$a_S = .01146T + 2.2537 \quad \textit{(longitudinal)} \tag{3}$$

$$a_S = .01646T + 1.8077 \quad \textit{(transverse)} \tag{4}$$

These values are plotted along with handbook data[4] in Figure 3. Both longitudinal and transverse CTE's are comparable to the handbook data, and serve to verify the method of strain gage application and readout. It can be seen that the actual data has some curve to it, while our curves are linear due to the 2nd order polynomial. This straight line fit to the data is sufficient for use as input to the FEA model.

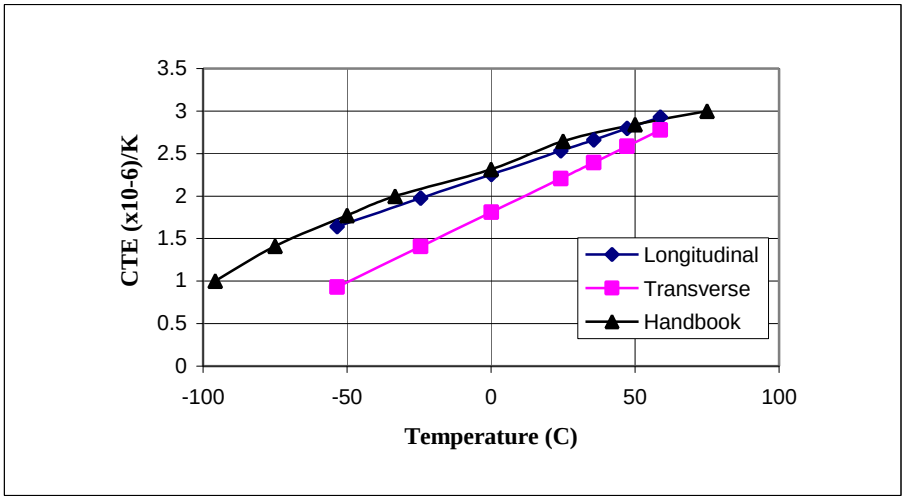

Figure 3: Silicon CTE's (strain gage method)

3. Tracker Tray Thermal Test

3.1 Test description

The thermal tests spanned temperatures in the operating range, the survival range, and rapid transients.The operating range comprised temperatures of 24, 30, 17, 35, 10, 40, 3, -4, and -10°C. The survival range comprised temperatures of 24, 50, 60, -20, -40, and -55°C. The transient test made three complete cycles between 40 and -55°C, starting at 40°C. Figure 4 shows the range of temperature for the three tests and the relative ramp rate for each test. (Note that the hold time at each temperature is not shown in Figure 4.) The ramp rate for the operational and survival temperature tests was held below 2°C/minute, while the transient test was performed with a 15°C/minute ramp rate. The purpose of these tests was to examine possible failure modes of the silicon detectors as they were bonded to the tracker tray. In addition, measured strains would be compared to predicted strains to validate the finite element (FE) models.

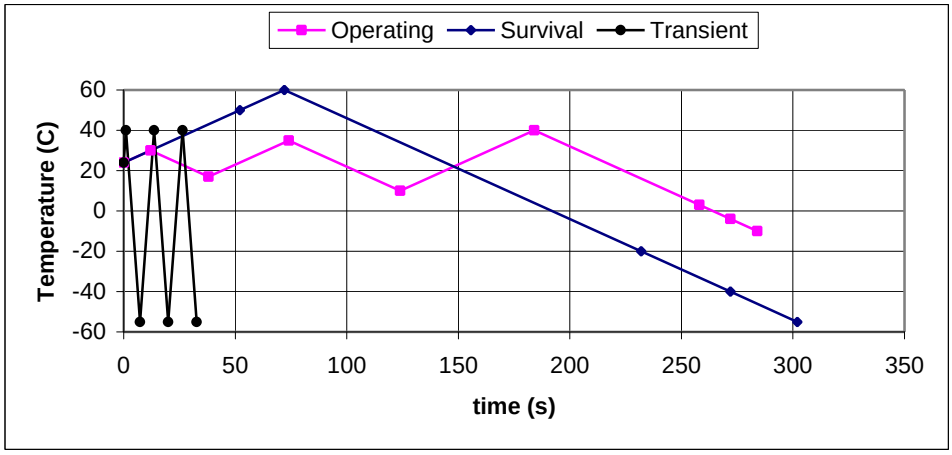

Figure 4: Temperature range for the three tests of the tracker tray

The individual silicon detectors on the tray were instrumented with strain gages and RTD's, as shown in Figure 5. Strain gages oriented parallel to the aluminum oxide strips in the silicon measure the longitudinal strain, while those perpendicular to the strips measure the transverse strain. The majority of the gages were installed on the bottom of the tray (4 transverse, 5 longitudinal, and 2 rosettes), but 2 transverse gages were installed on the top of the tray. In addition, a silicon detector instrumented with 1 resistance temperature device (RTD), 1 longitudinal, 1 transverse, and 1 rosette gage was placed in the oven to provide a reference for subtracting the thermal strain.

The tracker tray was built with an aluminum closeout frame at SLAC from drawings provided by HYTEC, Inc. The top and bottom layers were bonded to an aluminum core with 0.002" thick walls, and cell size of 0.375". The core is Hexcel CR111-3/8-5052-002P-3.0. Aluminum face sheets 0.002" thick were bonded to each side of the core, followed by a lead layer 0.008" thick bonded to the bottom only. Kapton/copper bias circuits 0.008" thick were bonded to the lead, followed by the silicon detectors. Three silver epoxy pads per silicon detector (as shown by the grey circles in Figure 5) hold the ladders to the bias sheet. For the tray test, detectors were placed as shown in Figure 5, with the remaining spaces having 6061 aluminum squares to simulate the weight of the detectors.

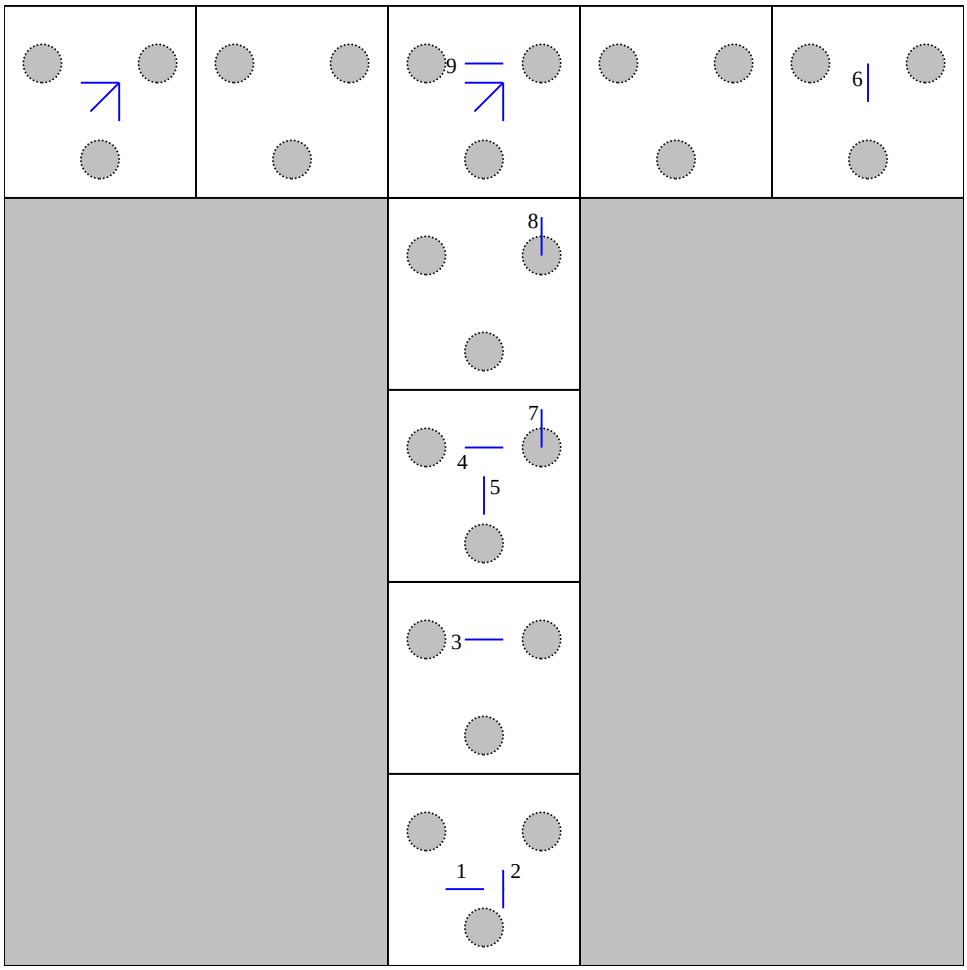

Figure 5: Strain gage layout on the tracker tray, showing epoxy bond locations

3.2 Strain results

The result of the testing was failure in two of the silicon detectors, as shown in Figure 6. Detector 1 (which had strain gages 1 and 2 attached), and Detector 3 (which had strain gages 4, 5, and 7 attached) each failed between the top of the detector and the two bonding pads. Following the operating and survival tests, the entire assembly was removed from the oven and examined carefully; no breakage or visible damage was noticed at this time, although it is possible that some de-bonding had occurred. The failure in both detectors therefore occurred sometime during or after the transient test, although it appears from the data that the silicon had de-bonded from some of the pads during the first two tests. Although it is not possible to say the specific temperature at which these de-bondings may have occurred, it appears that between –4 and –10, gage #9 experienced an unexpected stress relief.

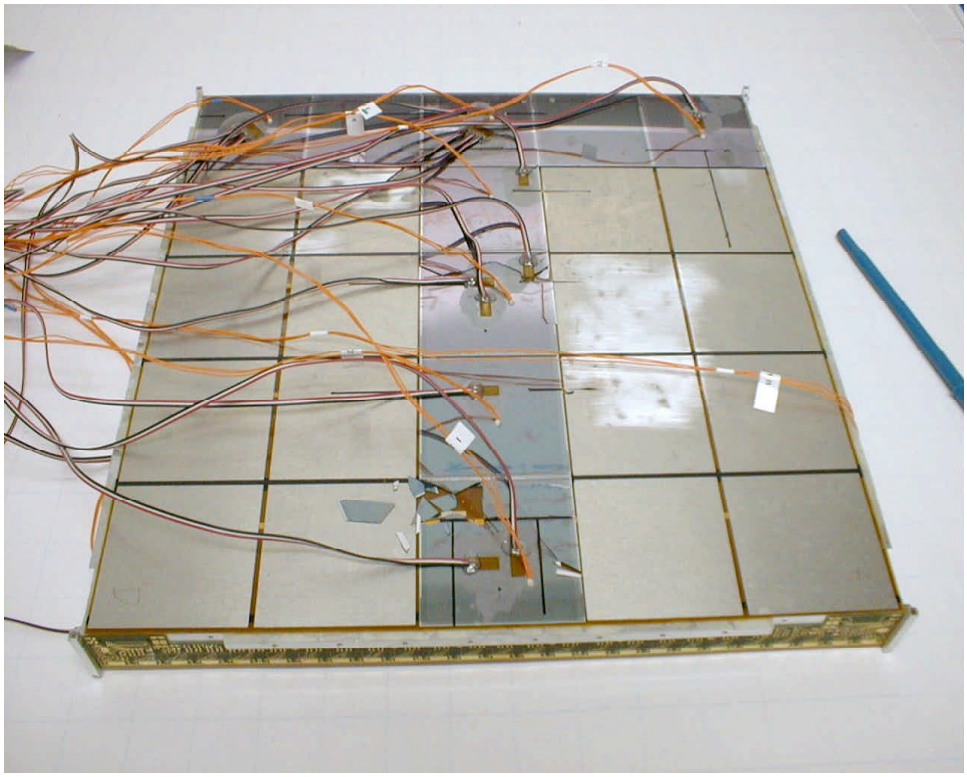

Figure 6: The tracker tray after testing. Note breakage on detectors #1 and #3

Test data is shown in Figure 7 (transverse strains) and Figure 8 (longitudinal strains). The first graph in each series shows the measured strain for the operating range test, which was performed first, followed by the survival range test, with the transient test last. The operating temperature test measured strains at 24, 30, 17, 35, 10, 40, 3, -4, and –10 °C. The survival temperature test measured strains at 24, 50, 60, -20, -40, and -55°C. The transient tests made three complete cycles between 40 and -55°C, starting with 40°C. The test number on the x axis correlates to a specific temperature given in the title of the graph. For example, in the top graph

of Figure 7, test #1 was at 24° C, test #2 was at 30° C, test #3 at 17° C, etc. The graphs in Figures 7 and 8 will be further interpreted in Section 3.5.

The values plotted in these graphs are the mechanical strains, as defined in the following equation, where total strain is the sum of mechanical strain plus thermal strain.

$$e = \frac{s}{E} + a\Delta T \qquad (5)$$

Mechanical strain is thus the result of the total measured strain of a gage located on a test tray mounted detector, minus the strain measured on a free piece of silicon at the same temperature. The free piece of silicon is referred to as the reference piece.

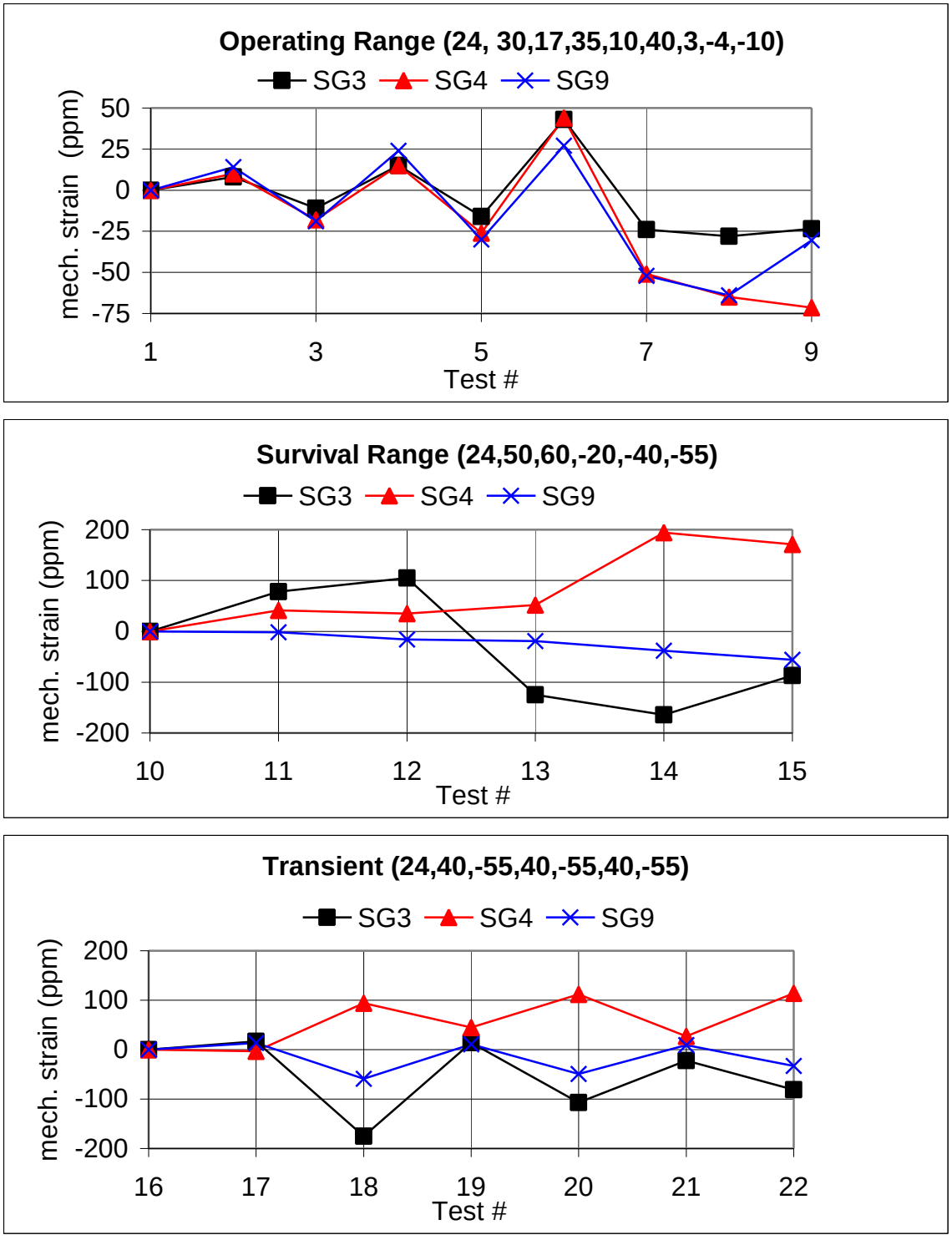

Figure 7: Operating, survival, and transient temperature test results for transverse gages

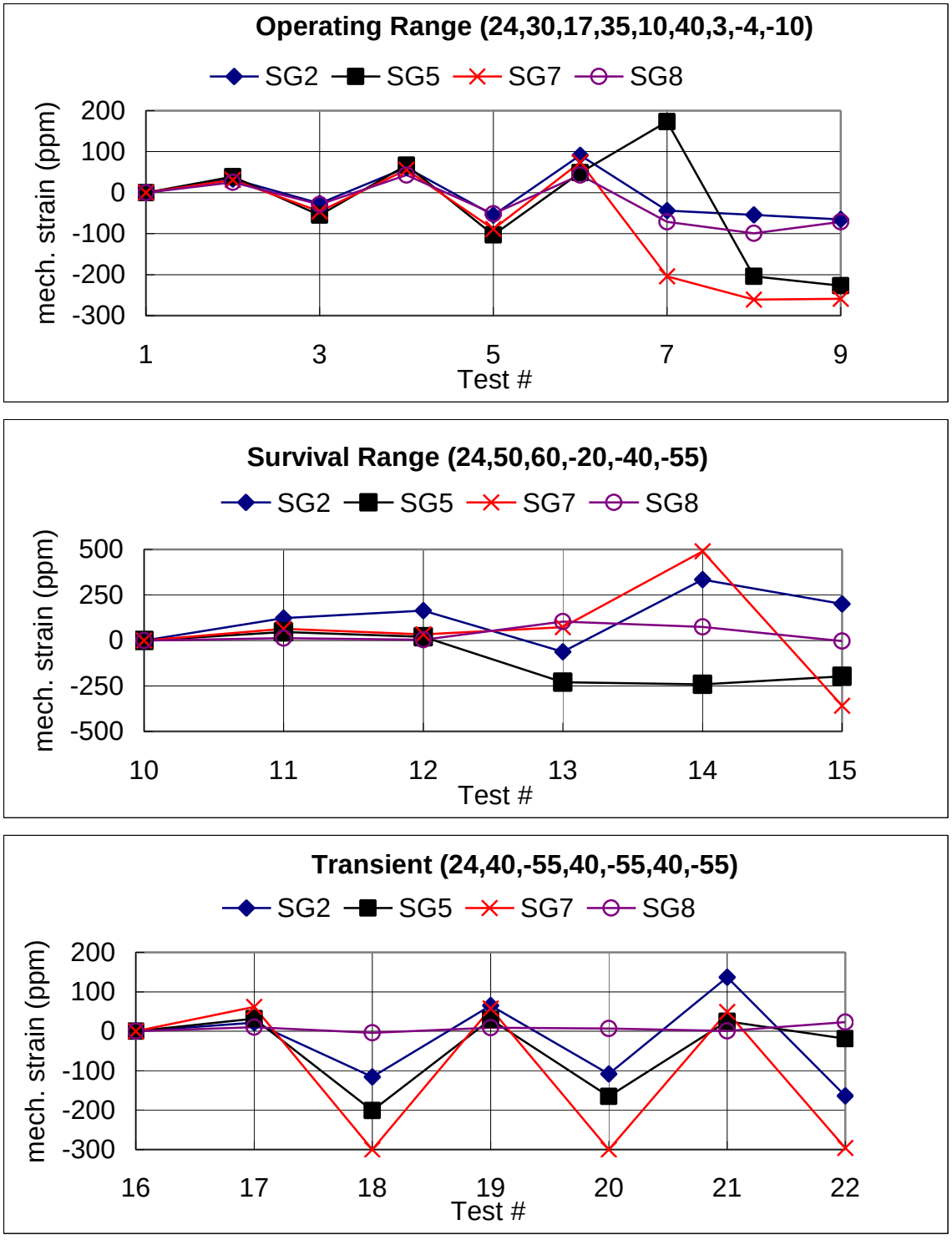

Figure 8: Operating, survival, and transient test results for longitudinal gages

3.3 Tracker tray thermal test FEA model

The finite element model for the GLAST thermal tray test was built using COSMOS/M version 2.5. Because the prototype GLAST tray closeout used for thermal testing was constructed with only one continuous silicon detector ladder, the finite element models reflect this design by modeling a single silicon detector ladder with boundary conditions that were representative of the rest of the tray closeout. 2-D and 3-D models were built. Plane2D elements were used to represent the payload layers of the silicon detector ladder through the thickness. Figure 9 shows the 2-D model case at the edge bond of two silicon detectors. One of the silver epoxy pads is shown at the far left of the figure.

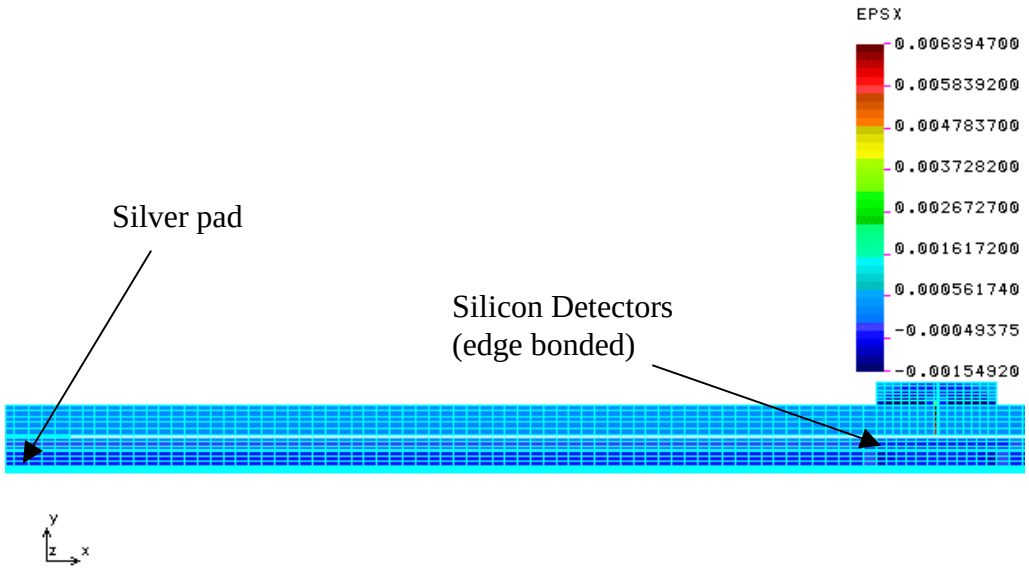

Figure 9: 2D COSMOS model at silicon edge bonds.

Shell4L, Solid, and Shell4 elements were used to represent the payload layers in the 3-D model. Shell4L elements represented the aluminum 6061-T6 face sheet, lead converter squares, Kapton/copper bias sheet, and the epoxy layers in between each. Solid elements represented the silver conducting epoxy used to bond the silicon detector ladders to the Kapton/copper bias sheet. Shell4 elements represented the silicon detectors and epoxy used for bonding at detector edges and between the detectors and kapton. All material properties used in the analysis are listed in GLAST document number HTN-102050-13[5].

A static-thermal loading condition was used to check how the coefficients of thermal expansion for the different materials in the payload share the load and stress the ladder. The bottom face of the aluminum face sheet was constrained to simulate connectivity to the tray closeout and tray closeout core. Figure 10 shows the 3-D model case.

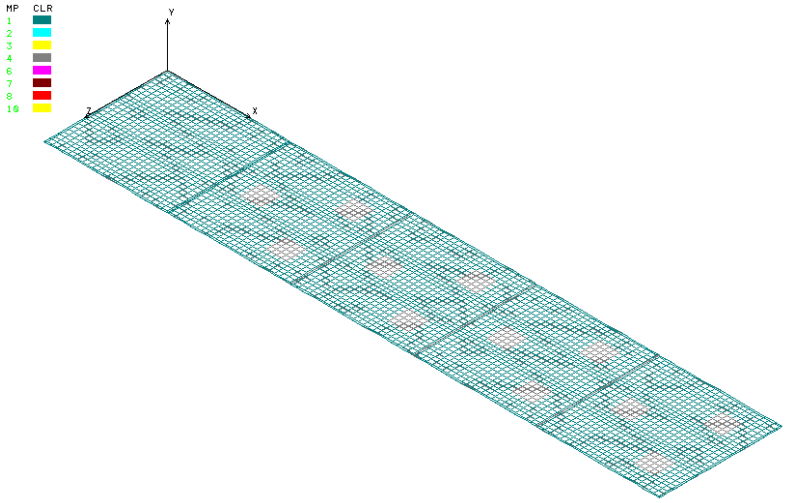

Figure 10: 3D COSMOS model showing epoxy pad locations

Strain values from the 2-D and 3-D models for each of the temperatures tested in the actual prototype tray test were determined and compared. Figure 11 shows the strain profile for the strain gage locations on the silicon detectors in the 3-D model case.

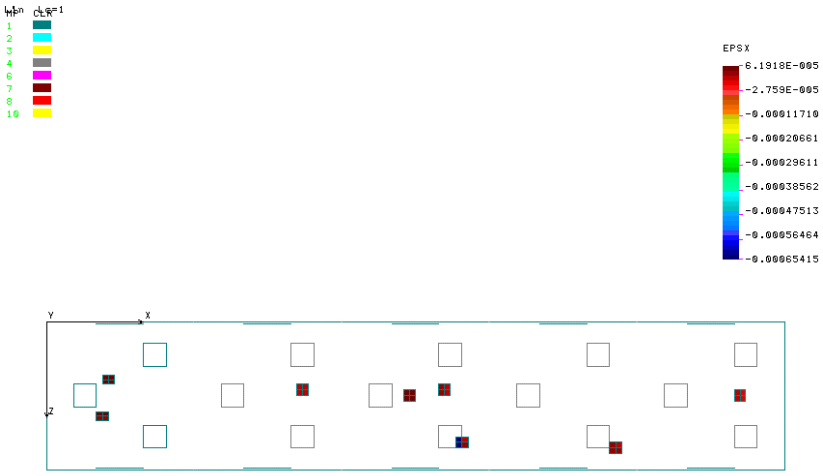

Figure 11: Predicted strain profiles at locations of gages

3.4 Measured results compared to FEA

The longitudinal and transverse results were predicted by a finite element model. The first order analysis models the tray assembly in 3 dimensions, but does not include the effects of the closeout. Using the model, strains were generated for each gage under thermal conditions corresponding to the physical tests. Strain measurements were taken at each gage when the oven temperature had been held at a given set point for at least twenty minutes. Between each of the

three tests, the strain readouts for each gage were re-zeroed at 24°C by re-balancing the measurement bridge. The measured strains were then adjusted by subtracting off the thermal strain, as discussed in Section 3.2. Figures 12-18 show the results of both the model and the data measurement.

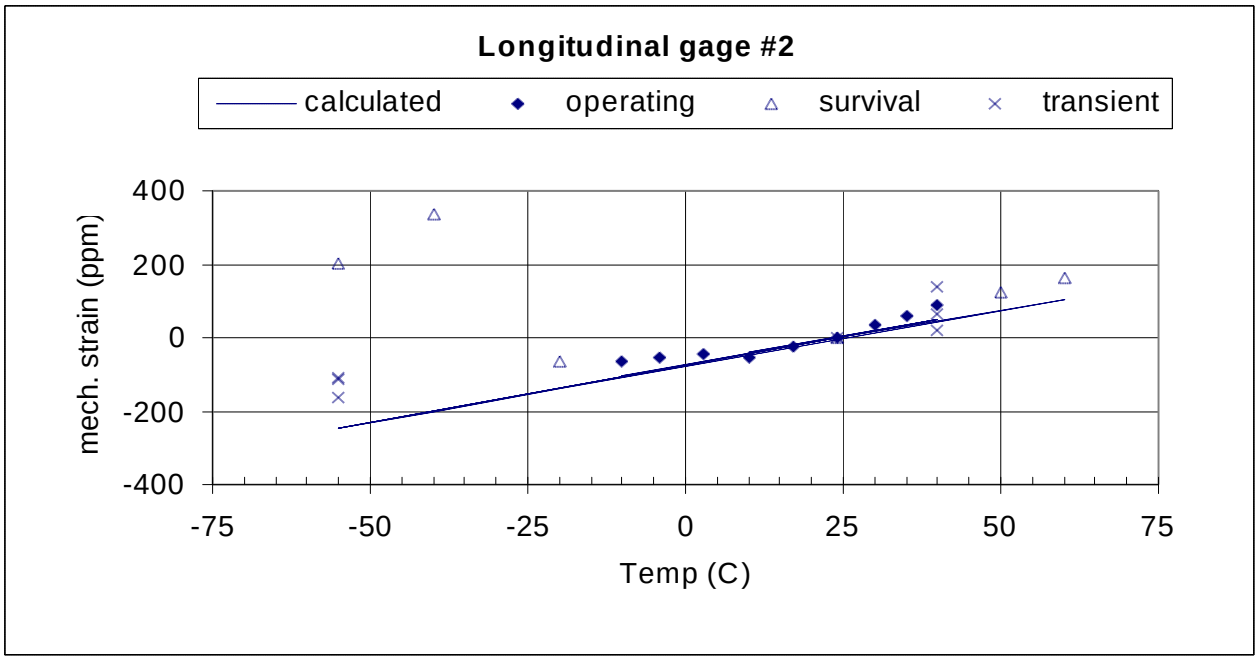

Figure 12: Measured and calculated strains, longitudinal gage #2

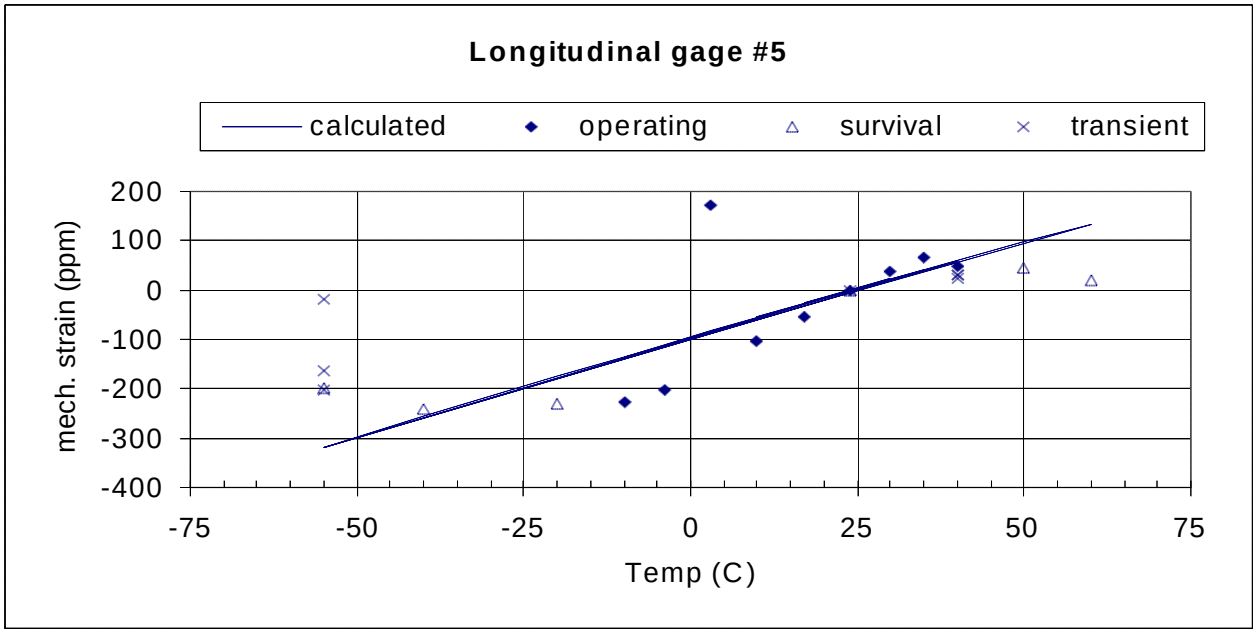

Figure 13: Measured and calculated strains, longitudinal gage #5

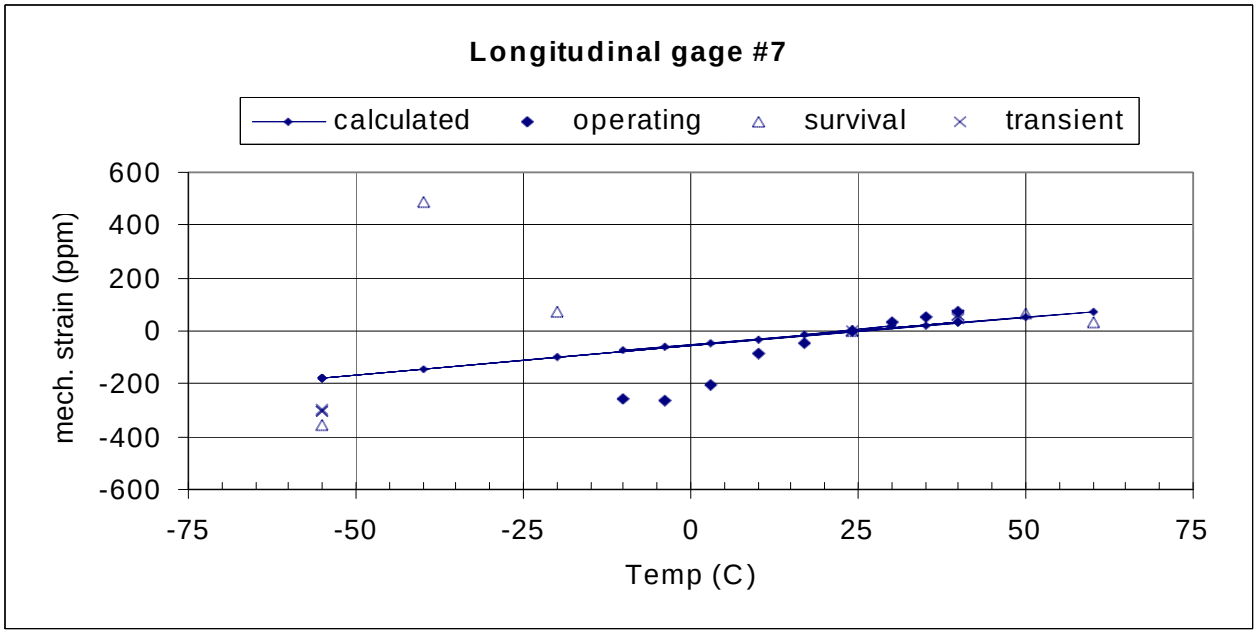

Figure 14: Measured and calculated strains, longitudinal gage #7

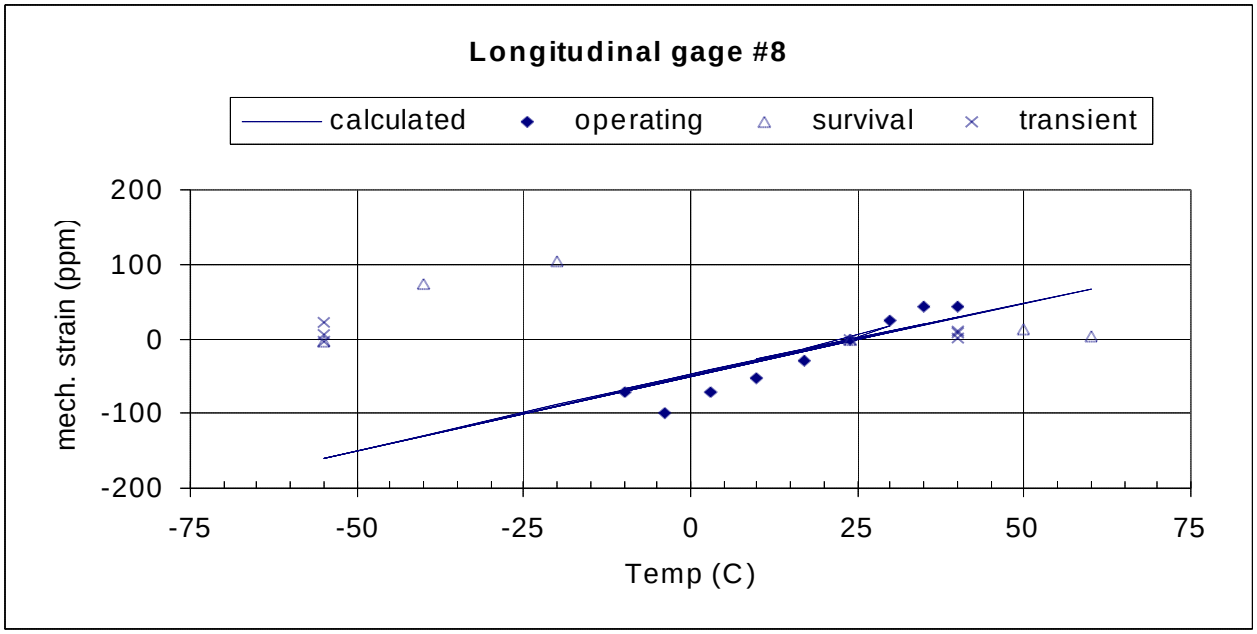

Figure 15: Measured and calculated strains, longitudinal gage #8

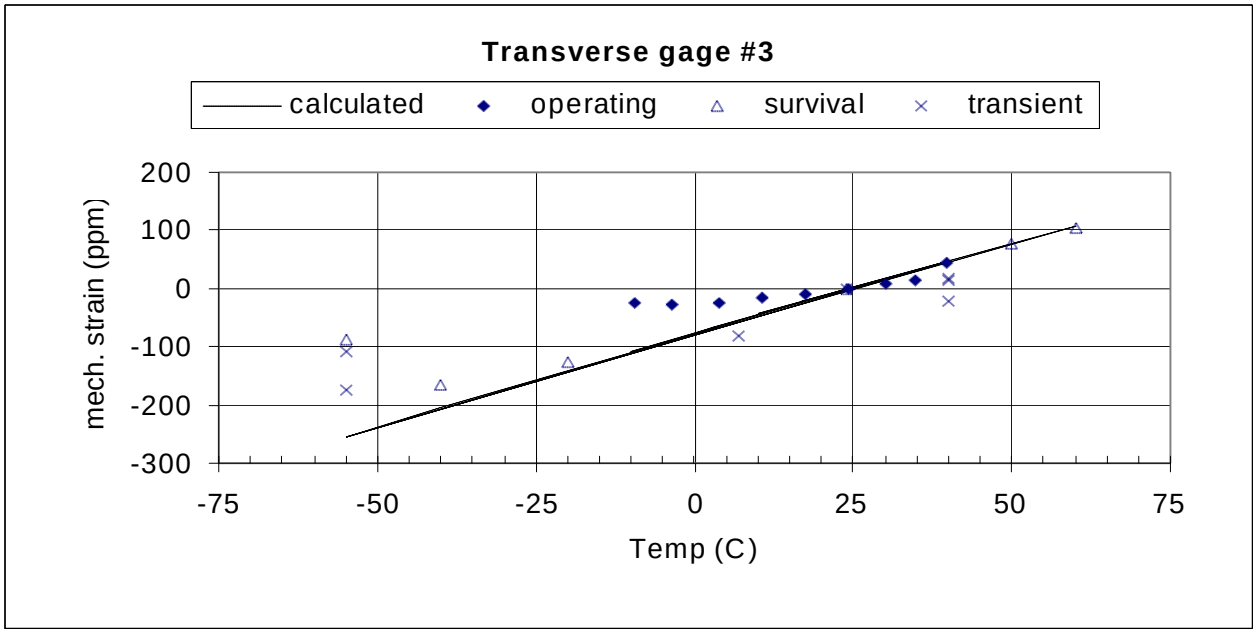

Figure 16: Measured and calculated strains, transverse gage #3

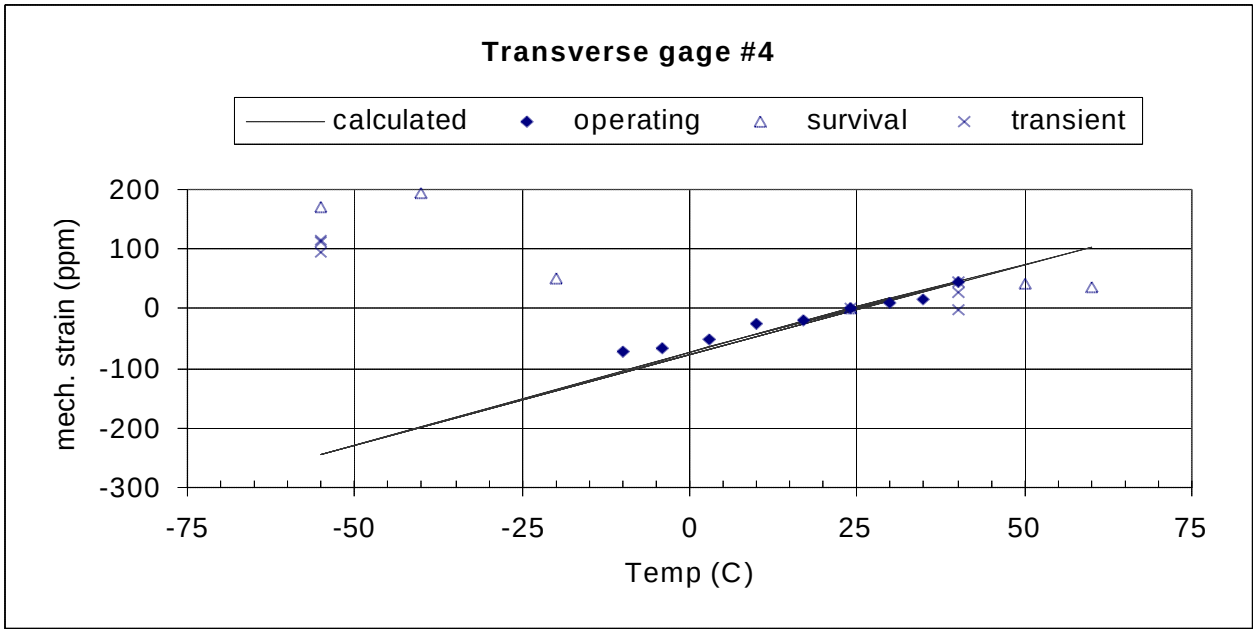

Figure 17: Measured and calculated strains, transverse gage #4

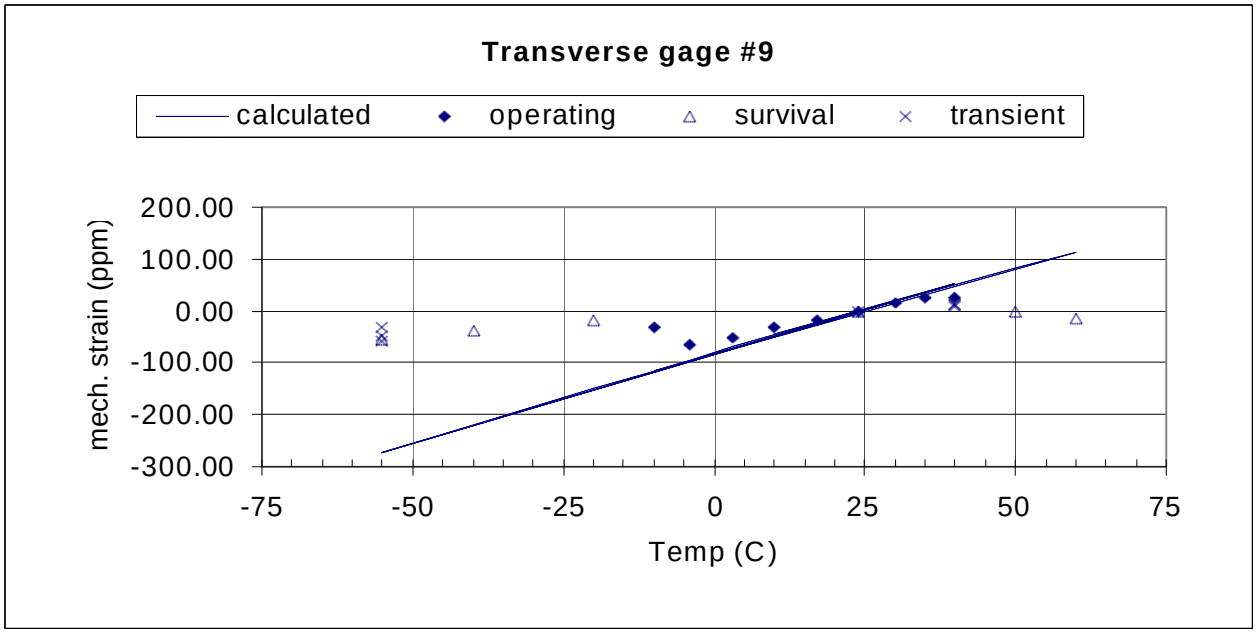

Figure 18: Measured and calculated strains, transverse gage #9

3.5 Results and discussion

Looking at the three graphs in Figure 7, it is apparent that something changes during the course of the testing. For example, gages #3, #4, and #9, which are located in similar areas in relation to the epoxy pads, show similar trends during the operating temperature test, but only gage #3 shows the expected trend during the survival temperature test. Gage #9 has almost zero strain, while gage #4 shows significant tensile strain. During the transient test, the trend is similar, with gage #3 showing expected trends, gage #4 the opposite trend from that expected, and gage #9 now shows the expected compressive strain, but of a much lower magnitude than gage #3. This could indicate de-bonding of some of the pads, and after disassembling the tray following these tests, it was apparent that all of the pads between gage #9 and #7 had de-bonded. De-bonding of the pads would probably not explain the tensile strain of gage #4 after the operating temperature test. It is possible that during the survival temperature test, the epoxy exceeded the glass transition temperature during the 50 and 60° C tests. Cured epoxy reverts to a soft material at the glass transition temperature, and must be re-cured to become hard. The manufacturer of the epoxy used to bond the detectors identifies the glass transition temperature at 52°C. The epoxy would then re-cure at lower temperatures, and induce some residual strain. This effect will be further discussed in Section 3.5.

The same general effects seem true of the longitudinal gages, results of which are plotted in Figure 8. All the longitudinal gages show similar trends during the operating range tests, with the exception of gage #5 at the 3°C temperature. This gage returns to the expected strain direction after the 3°C test. However, during the survival range test, gages #2, #7, and #8 show tension after the 60°C test, indicating that a change occurred at that temperature.

These trends are perhaps more clearly seen in Figures 11-17. In these figures, the calculated results have been plotted along with the measured results, and each of the three

temperature test ranges are easily distinguishable. The measured results are all fairly close to the predictions for the operating temperature test range. The major discrepancy between the model and the data for this temperature range occurs consistently at temperatures near and below 0°C, and is true for both the longitudinal and transverse gages. In general, the calculated values have less slope than actually measured; i.e, the data shows more strain per degree of temperature change than is being predicted. This discrepancy could largely be accounted for by incorrect material properties used in the model, or because of the effect of the closeout tray, which was not included in the model. It is very apparent, though, that during the survival and transient tests, the measured values are in general much farther from the predicted values than during the operating temperature test. This effect is due to failures of some type. For the longitudinal gages, #'s 2, 7 and 9 show a large deviation from the predicted value during the survival temperature test, especially at the –40 and -55°C points. Again, this effect could be due to de-bonding or the glass transition temperature, but it is difficult to reach a qualitative conclusion about the actual method of failure.

Interpretation is helped somewhat by examining the tray after testing. For convenience, we number the silicon detectors of interest from #1 to #5, with #1 being at the bottom of the "T" in Figure 6, and #5 at the top of the "T". Figure 19 shows the catastrophic failure that occurred on detector #1, and it is apparent that at least the bottom pad on detector 2 had de-bonded. Figure 20 shows the catastrophic failure on detector #3, and again it is apparent that de-bonding has occurred on all the bonds on detector 4. Both fractures occurred at the top of a detector, adjacent to the two epoxy pads at the top of the detectors. Figure 15 gives a typical example of the results of all the gages; fairly linear results during the operating range of temperatures, essentially zero mechanical strain during the 50 and 60°C tests, (because of the glass transition temperature), followed by high values of tensile mechanical strain at the low temperatures of the survival range of tests. This tension occurred in gages three of the four longitudinal gages (#'s 2,7, and 8), but is not easily explained. During the transient tests, the mechanical strain is essentially zero again, probably because of the detector failure shown in Figure 20. Following the glass transition temperature, the epoxy would re-harden at lower temperatures, which would induce larger than expected compressive stress at low temperatures, possibly causing the de-bondings. The catastrophic failures then occurred during the first or second cycle of the transient test. The unknown in this sequence is what effect the de-bondings have on the measured strains, and can this explain the large tensions mentioned above.

It does appear that the additional expansion that is allowed when a pad de-bonds contributes to the failure, because the detectors can bend out of plane by a much farther amount than when they are restrained by the bonding pads.

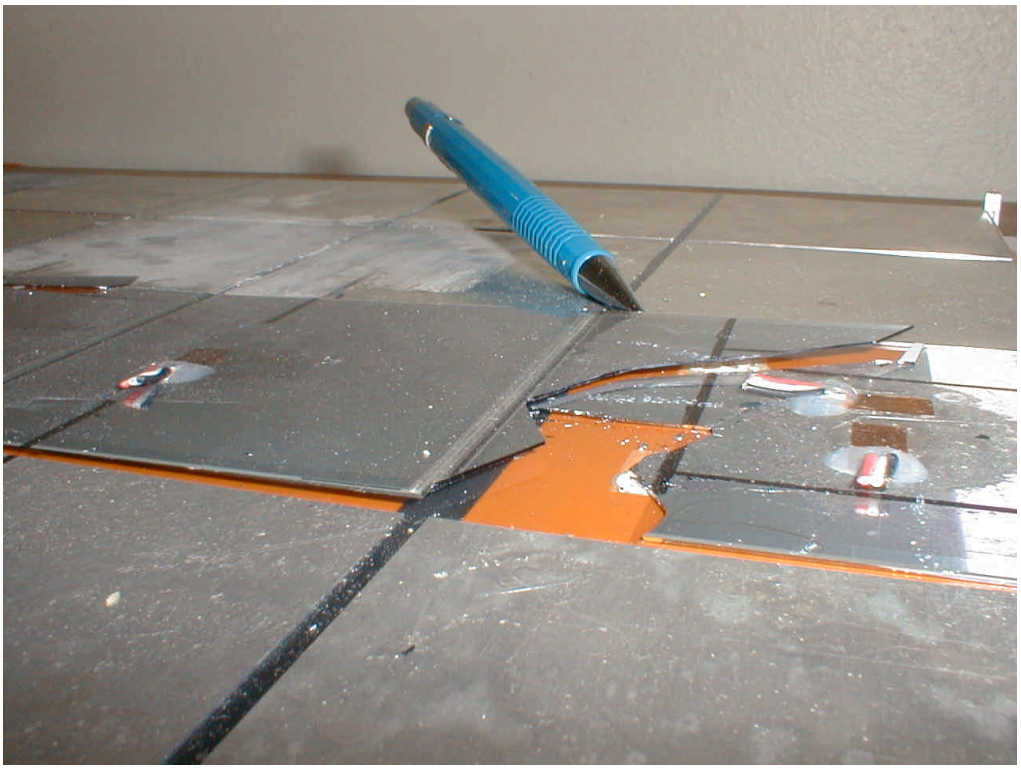

Figure 19: The break in silicon detector #1. The black line across the broken area denotes the location of the two epoxy bonding pads

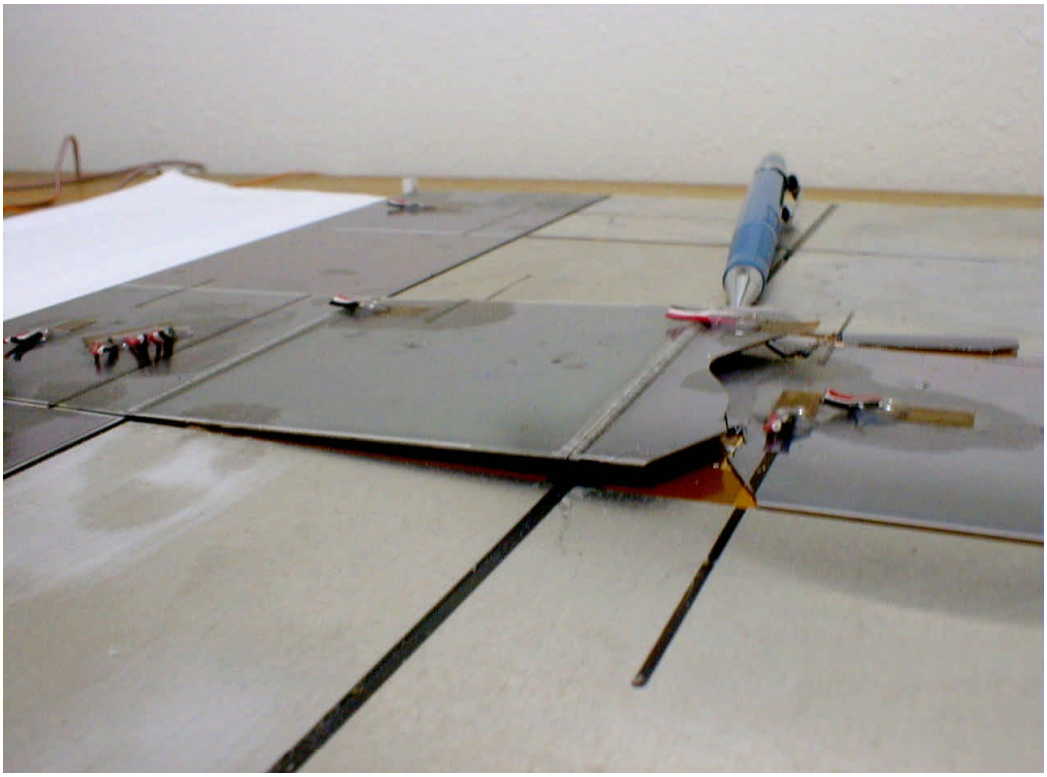

Figure 20: The break in silicon detector #3. The black line across the broken area denotes location of the two epoxy bonding pads.

4. Ladder Tests

These tests were performed to compare aluminum and carbon face sheet materials. Four different GLAST payload coupons were tested simultaneously. Each ladder was actually made up of three individual silicon detector strips that were edge-bonded together to simulate the actual tray construction. The variations between the four ladders were the thickness and material of the face sheets, and the thickness of the lead converter layer. Ladder #1 had a 12 mil quasi-isotropic Gr/CE face sheet with 8 mil lead converter. Ladder #2 had a 3 mil woven Gr/CE face sheet and 8 mil lead converter. Ladder #3 had a 2 mil aluminum face sheet and 8 mil lead converter. Ladder #4 had a 12 mil quasi-isotropic Gr/CE face sheet with a 61 mil lead SuperGLAST converter. All four ladders had the same thickness for the silver-epoxy pads, bias circuit, and silicon detectors. A voltage was applied to the kapton layer, and the leakage current was monitored for positive indication of a silicon failure. This current loop was through three of four ladders, and so a short circuit indicates only a failure in the silicon, but not the location of the failure.

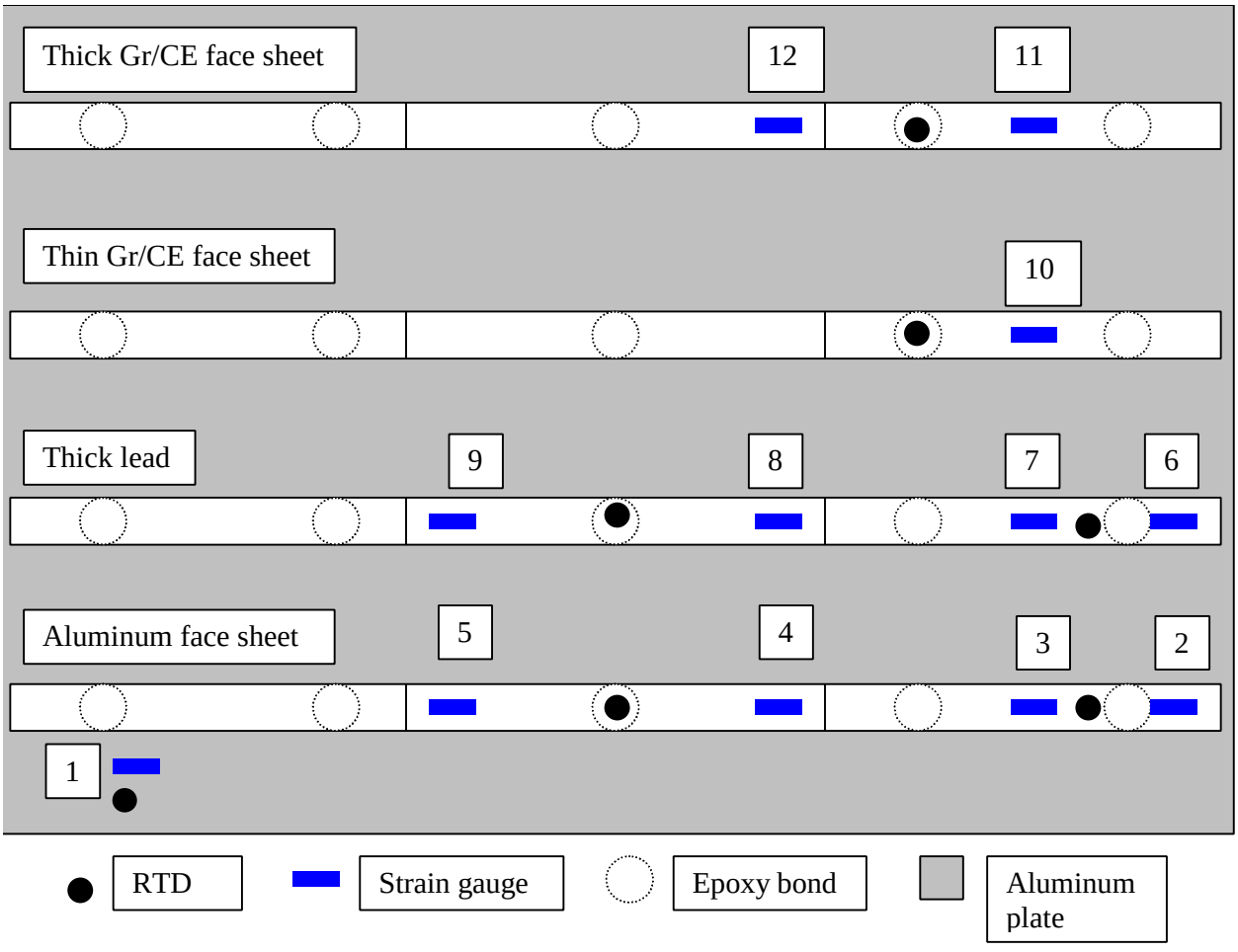

Figure 21: Ladder test instrumentation

The silicon was bonded to kapton in five places, as shown in Figure 21. The ladders were bonded to a honeycomb layer, that was in turn bonded to a 1” thick aluminum tooling plate. The

strain gages were arranged as shown in Figure 21. The tests were similar to the tracker tray tests, with temperatures covering the operating and survival temperature ranges. The operating range test comprised temperatures of 24, 30, 17, 24, 40, 5, 24, -3, and -10°C. The survival test comprised temperatures of 24, 50, 60, 24, -15, and -23°C.

The tests resulted in failures in ladders #1, #2 and #4. De-bondings also occurred in each of the ladders.

4.1 Strain and test results

Figures 22, 23, and 24 show the overall test results, with temperature, current and strain as a function of time. It can be seen on the graph of current that a failure occurred sometime after 1600 minutes, between the –15 and –23 °C tests. The actual failure occurred at about -21°C, although the test setup did not allow identification of the location where the failure occurred.

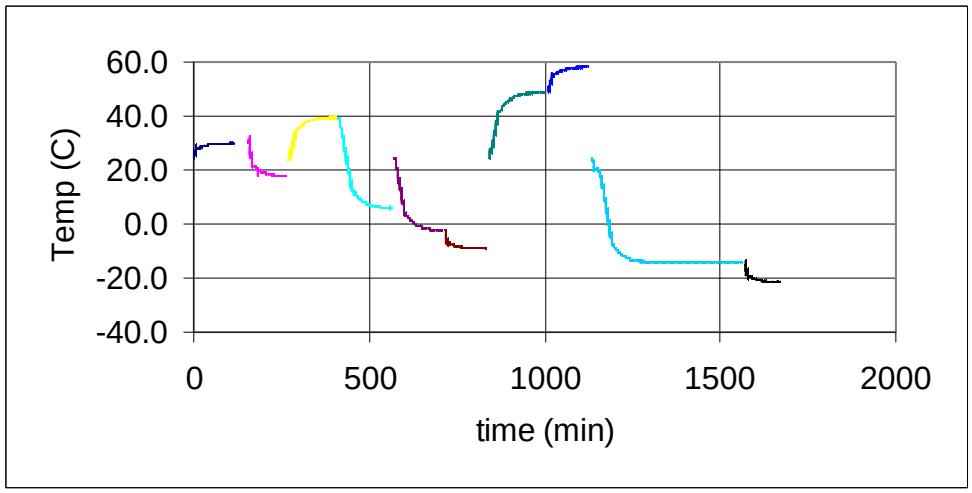

Figure 22: Temperature vs. time for the ladder tests

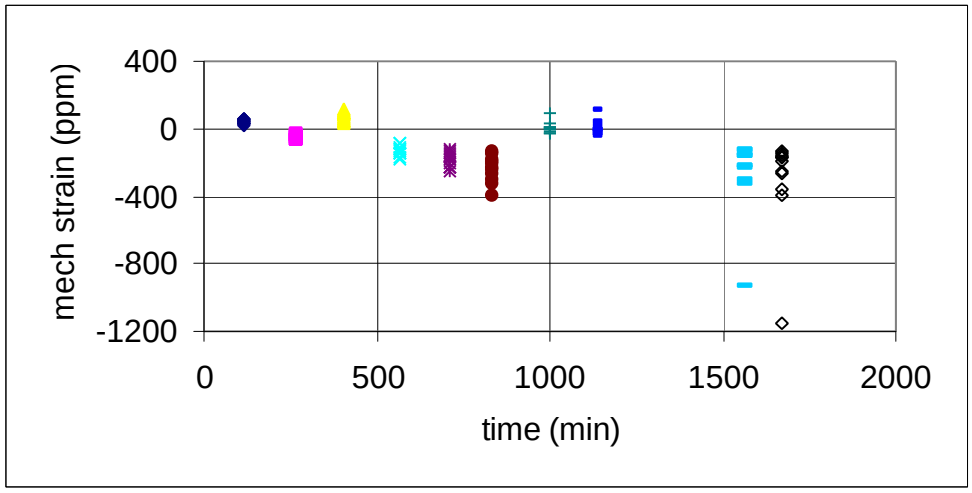

Figure 23: Strain from 12 gages vs. time for the ladder tests

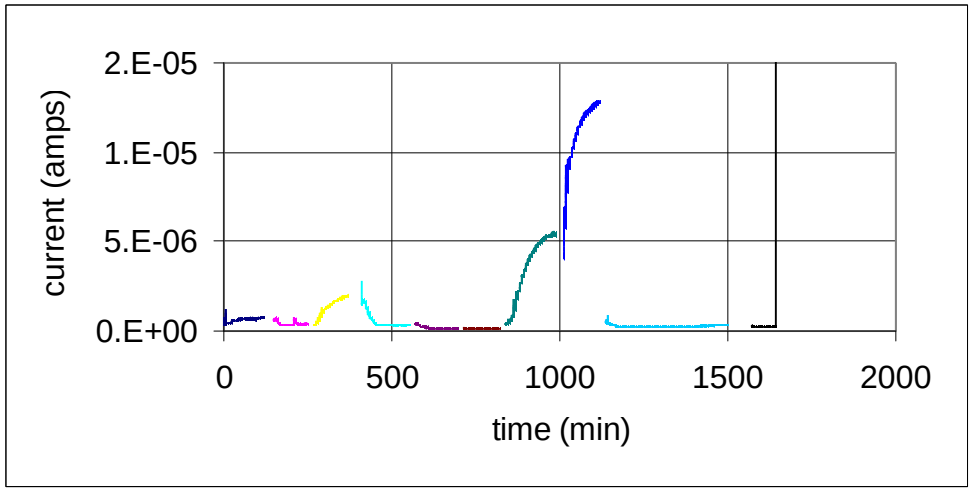

Figure 24: Current vs time for the ladder tests, showing short circuit at about 1600 min

The major point of this test was to evaluate the effect of different face sheet materials on the mechanical strain of the silicon. It can be seen from Figures 25 and 26 that there is very little difference in the measured strain. This is primarily due to the overshadowing effect of the aluminum plate to which the honeycomb was attached, which will be discussed in Section 4.4.

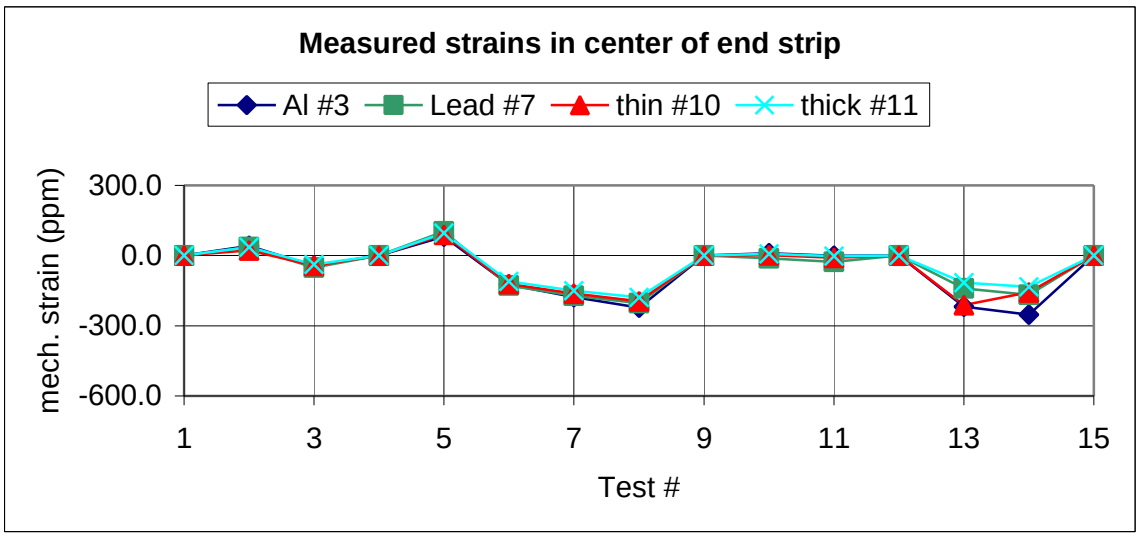

Figure 25: Measured strains at the same location (between two bonding pads) on the four different ladders

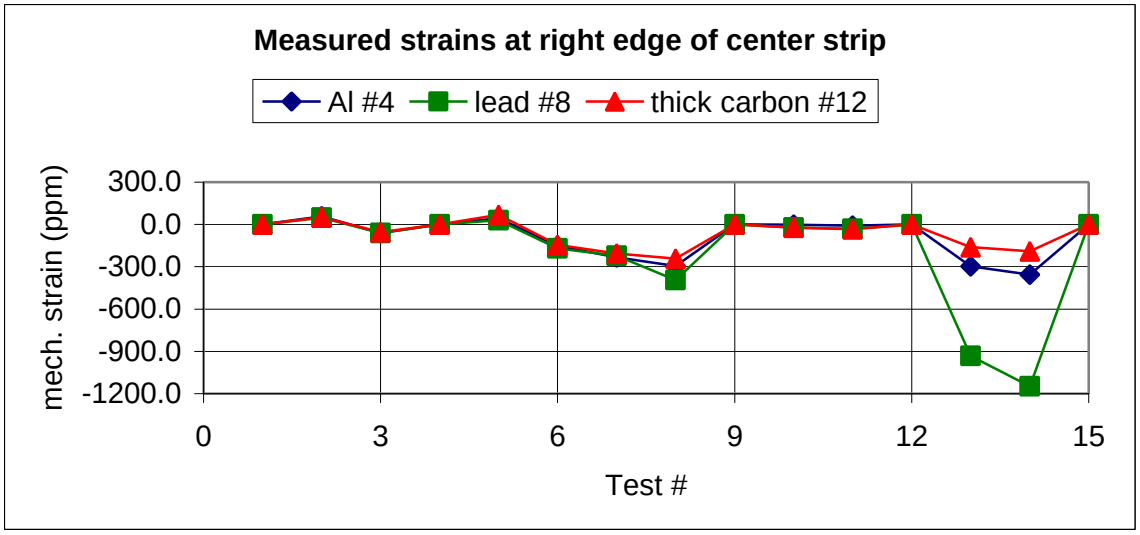

Figure 26: Measured strains at the same location on the four different ladders

4.2 Ladder test FEA model

The finite element model for the GLAST thermal ladder test was built using COSMOS/M version 2.5. Three 3-D models were built for the ladder test: One full model with the entire test set-up, (although the honeycomb was simply modeled as a layer having the properties of honeycomb supplied by the manufacturer) another that included only the payload ladders, and no aluminum honeycomb or tooling plate, and a third with a single ladder and the aluminum honeycomb in full detail attached to the tooling plate. The payloads for the GLAST ladders used the same elements as was done in the ladder for the 3-D tray model. All material properties used in the analysis are listed in GLAST document number: HTN-102050-13-DRAFT. Figure 27 shows the full 3-D model case with solid elements to represent the honeycomb and the tooling plate.

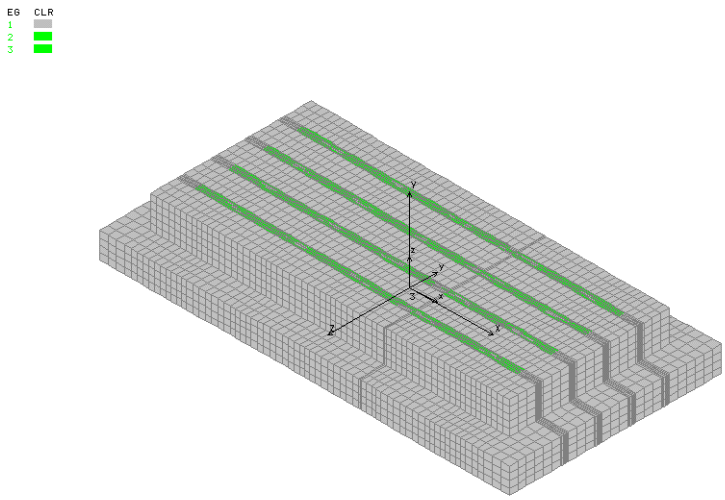

Figure 27: 3D COSMOS model with ladders, honeycomb, and tooling plate

A static thermal loading condition was used to check how the coefficients of thermal expansion for the different materials in the payload share the load and stress the four ladders. Boundary conditions were placed on the bottom face of the aluminum tooling plate to constrain the full 3-D model and the 3-D model of a single ladder from vertical translation. The 3-D model of the four ladders without the tooling plate and the honeycomb was constrained along the bottom face of the face sheet material for each ladder. Figure 28 shows the 3-D model of the four ladders without the tooling plate and honeycomb, and Figure 29 shows the 3-D model of a single ladder with detailed honeycomb.

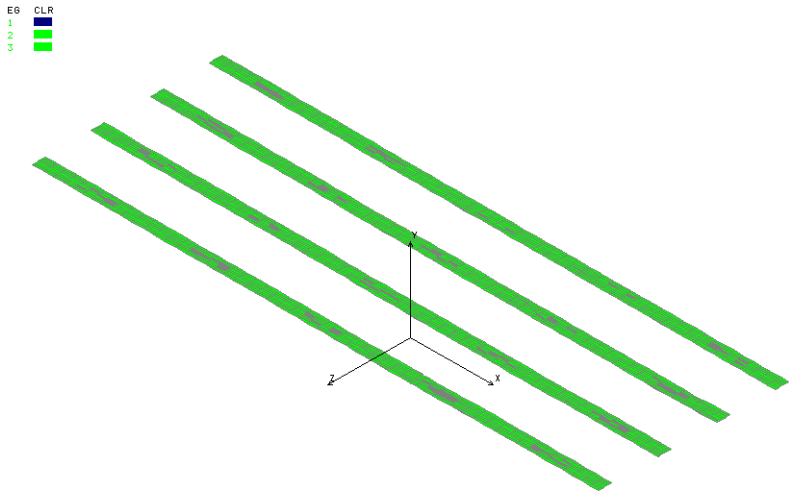

Figure 28: 3D model of ladders without honeycomb or tooling plate

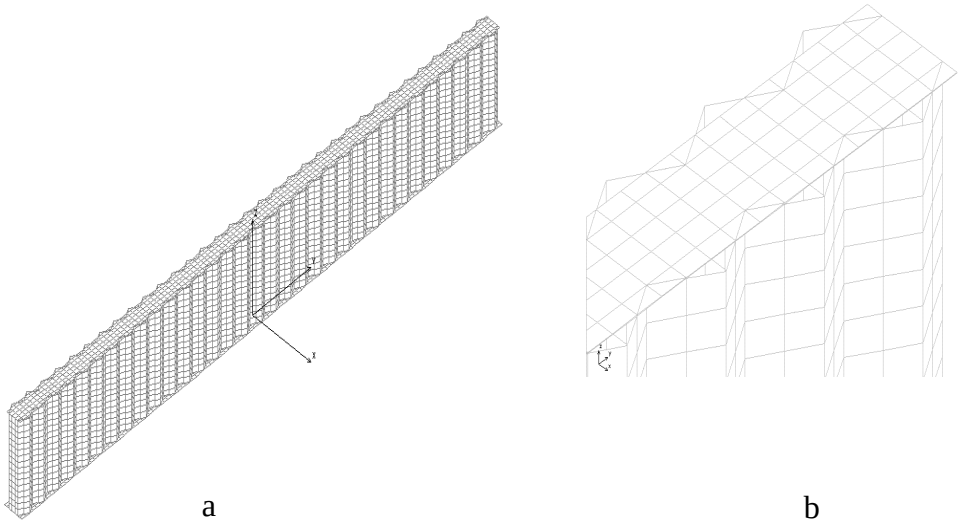

a b

Figure 29: 3D detailed model of ladder bonded to honeycomb; a) overall model, b) detail

Strain values from the 3-D models for each of the temperatures tested in the actual ladder test were determined and compared. Figures 30 and 31 show examples of the strain profiles for the ladders in the four-ladder 3-D model case and the single ladder 3-D model case, respectively.

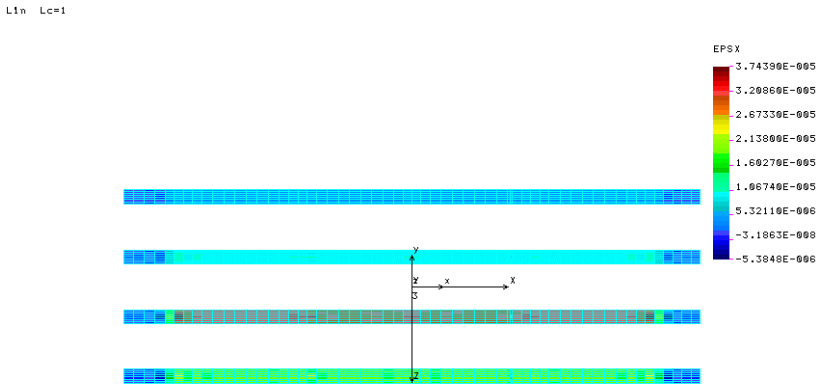

Figure 30: Example of strain profiles in the four ladders using the model with honeycomb and tooling plate.

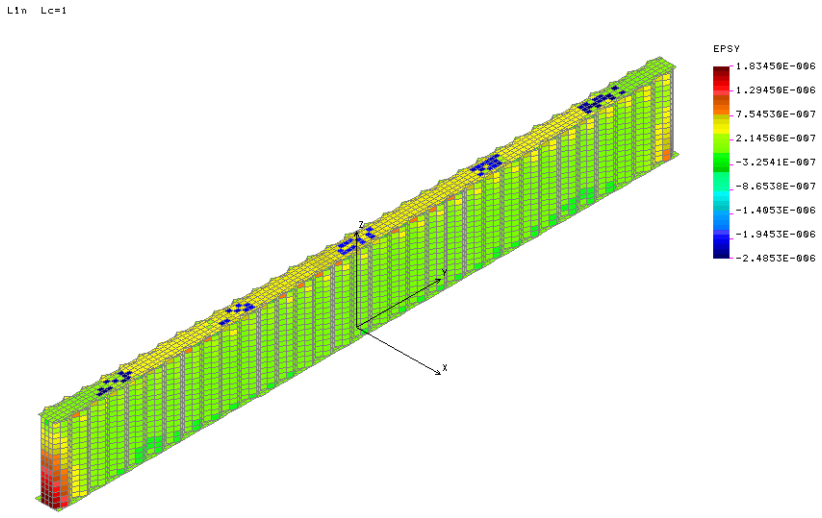

Figure 31: Example of strain profiles in a ladder using the detailed model of the honeycomb.

4.3 Measured results compared to FEA model

The mechanical strain is plotted along with the results of the model for selected gages. Once again, the mechanical strain is the total strain measured on the ladder minus the thermal strain measured on a free piece of silicon. The graphs show results from the model that included the honeycomb and the 1" thick aluminum plate.

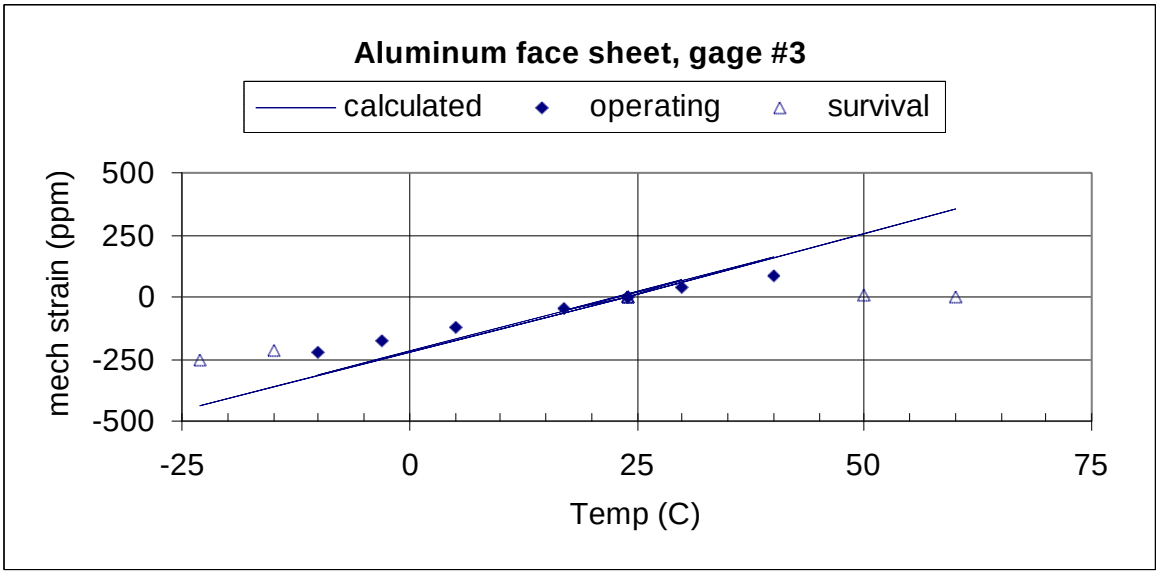

Figure 32: Measured and calculated strain results on aluminum face sheet ladder, gage #3

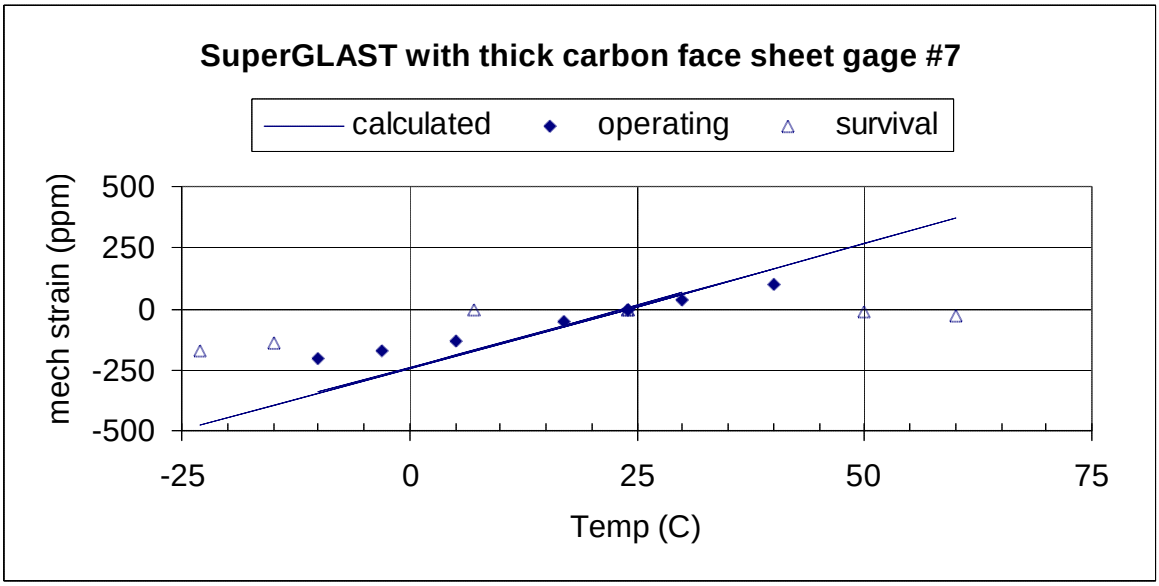

Figure 33: Measured and calculated strain results for ladder with thick carbon face sheet and SuperGLAST lead, gage #7

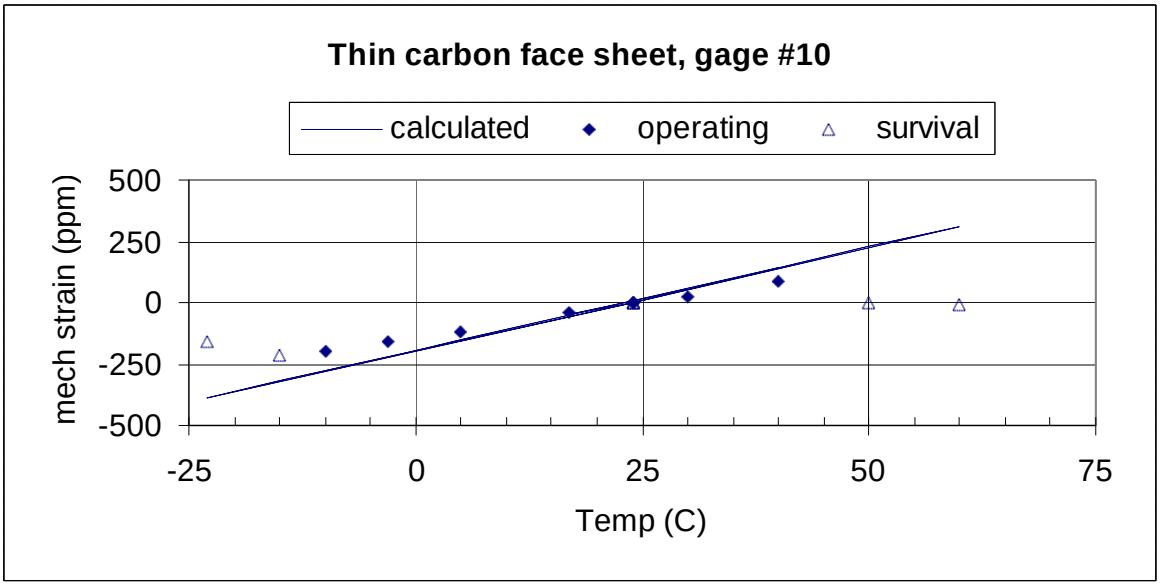

Figure 34: Measured and calculated strain results for ladder with thin carbon face sheet, gage #10

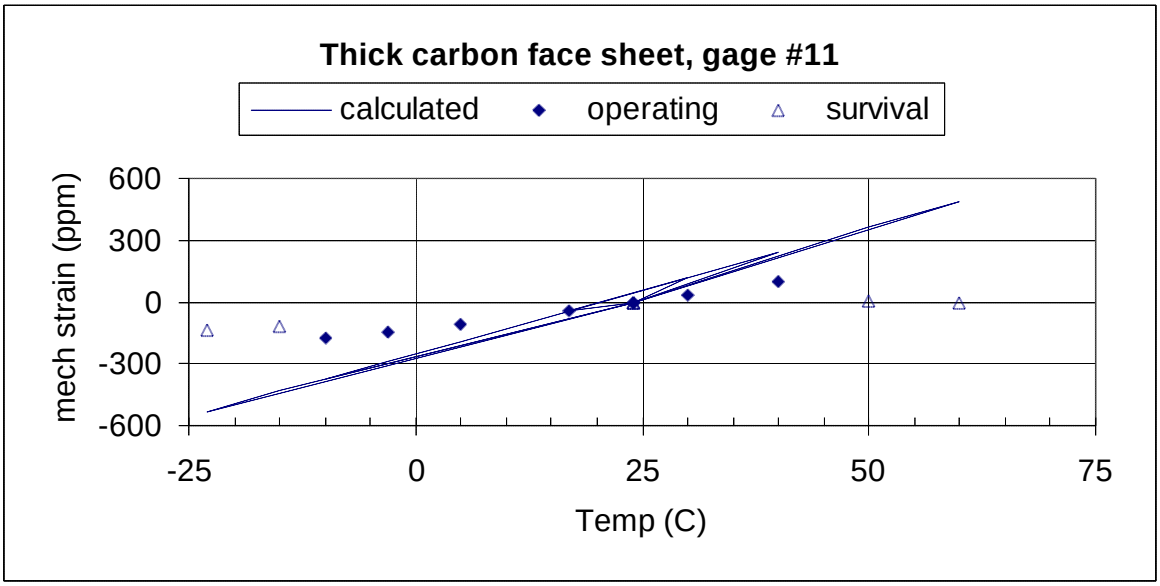

Figure 35: Measured and calculated strain results for ladder with thick carbon face sheet, gage #11

4.4 Results and discussion

It is apparent from Figures 25 and 26 that the different face sheet materials and the thick lead of the SuperGLAST layup had minimal effect on the overall strain in these tests. This is attributed to the expansion of the aluminum tooling plate, which was transferred through the honeycomb to the ladders. Because the tooling plate is much thicker than the ladder components, this effect overshadowed much of the static response of the individual ladders. Figures 32 through 35 show results of the simulation compared to measured data from a gage located between the two bonding pads on the end detector of each of the different ladders. It should be

pointed out that the model used to develop Figures 32-35 includes the full shear properties of the honeycomb provided by the manufacturer. In reality, it is expected that because the ladders were only mounted over partial segments of the honeycomb, the full shear transfer is not realized. Notice that the data in each case shows an almost linear relationship between strain and temperature, at least for the operating temperature test. This slope is less than the slope predicted by the model. This agrees qualitatively with the argument that the simulation is over-predicting the strains because the ladders are mounted on the honeycomb in such a way that only a fraction of the manufacturer's quoted shear transfer occurs. The detailed model shown in Figure 31 included local effects and the results of this model are plotted in Figure 36. This model shows good agreement with the measured data in the operating temperature range. It is expected that this model would give the same good agreement for all the gages, but due to time constraints the additional simulations for the other gages was not done.

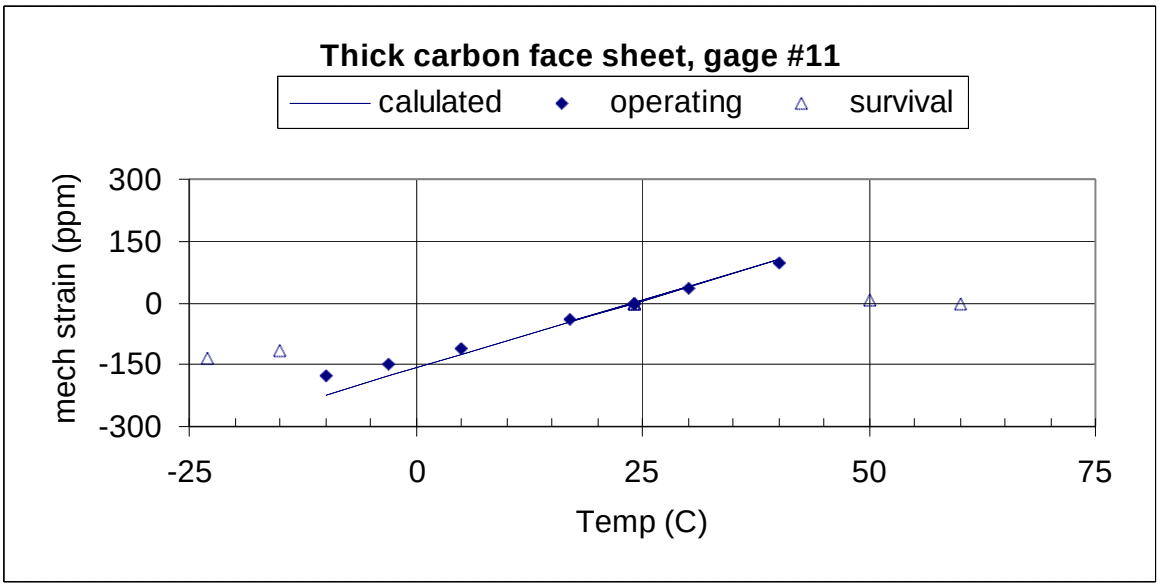

Figure 36: Measured and calculated strain results for ladder with thick carbon face sheet, gage #11. The calculated curve is based on a model that simulates the actual bonding method of the ladder to the honeycomb material.

As with the tray tests, it is apparent that significant changes occur during the survival temperature test. This test went from 24°C (the reference temperature) to 50°, 60°, then back to 24° and down to -15° and -23°C. The graphs in Figures 32-35 show that in each case, the measurement at 50° is much less than the expected strain, and that the measurement at 60° showed almost zero change in strain for the 10°C change in temperature. In fact, gage #11 shows almost zero strain at the 50 and 60°C temperatures. There are at least three possibilities: 1) the epoxy pads de-bonded in enough places to isolate the silicon from the ladders, or 2) a catastrophic failure occurred in the silicon or, 3) the epoxy reached the glass transition temperature allowing the silicon to freely expand. The measurement of the leakage current clearly showed that no catastrophic failures occurred until -21°C, and examination of the ladders after the tests showed that one de-bonding occurred in each ladder. The epoxy manufacturer specifies a glass transition temperature of 52°C, so this is a reasonable explanation for the zero

strain readings at 50 and 60°C. We expect that the epoxy would re-cure as the temperature dropped. For example, Figure 32 (aluminum face sheet) shows that the –15 and -23°C temperature test strain results fall right in line with the expected trend based on the operating temperature strains. Figures 33-35 show that this is not true for the other three ladders, which all showed strains less than expected for the -15 and -23°C tests.

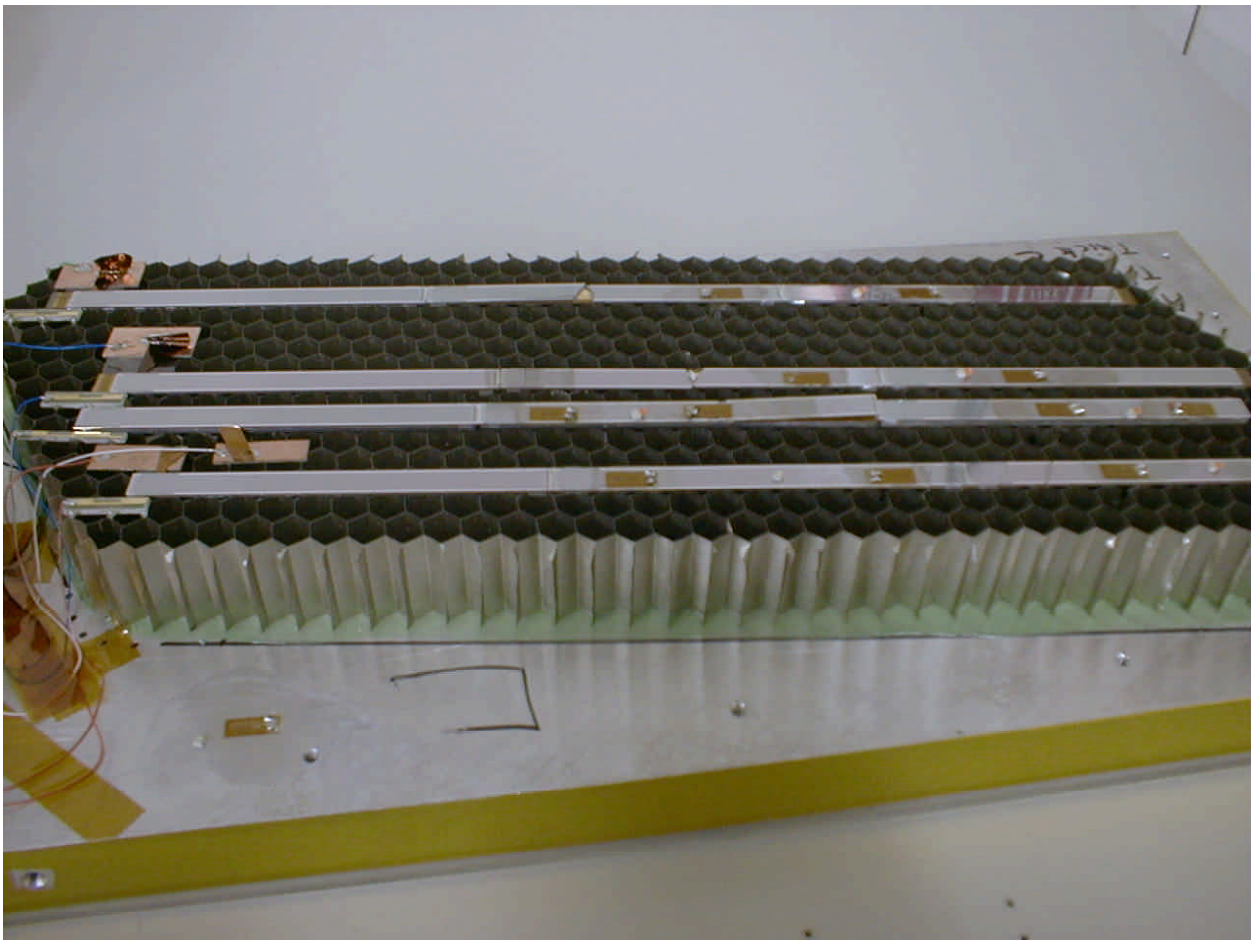

Figure 37: The four ladders after testing. Note the broken detectors on 3rd and 4th ladder from front (thin and thick carbon face sheets, respectively) and separation of the wire bonding between the right and center sections on the 2nd ladder from the front (thick lead face sheet).

5. References

[1] Tracker tray thermal test plan, HYTEC-TN-GLAST-12

[2] GLAST Science Instruments-Spacecraft Interface Requirements Document, August 3, 1999.

[3] "Measurement of Thermal Expansion Coefficient Using Strain Gages", Vishay Measurements Group Tech Note #TN-513-1. Measurements Group, Inc. PO Box 27777, Raleigh, NC 27611

[4] Electronic Materials Handbook, Volume 1: Packaging , p. 305: ASM International, November, 1989

[5] GLAST material properties document, HTN-102050-13